Modelling Engineered Barriers for Spent Nuclear Fuel Repository using a Double Structure Approach for Pellet based Components

Erdem Toprak[1], Sebastia Olivella[2] and Xavier Pintado[3]

[1] International Center for Numerical Methods in Engineering (CIMNE)
Universidad Politécnica de Cataluña
Campus Norte UPC, 08034 Barcelona, Spain
E-mail: erdem.toprak@upc.edu

[2]Department of Geotechnical Engineering and Geosciences,
Universidad Politécnica de Cataluña
Campus Norte UPC, 08034 Barcelona, Spain
E-mail:sebastia.olivella@upc.edu

[3]Saanio & Riekkola Oy, Laulukuja 4, 00420 Helsinki, Finland
E-mail:xavier.pintado@ains.fi

Abstract

Bentonite pellets are intended to be used as filling material in spent nuclear fuel repositories. The bentonite pellets can be used in gaps between the compacted clay blocks and the rock walls. Pillow pellets manufactured with MX-80 bentonite are intended to be installed in buffer between compacted blocks made with bentonite clay and the host rock. In addition, compacted clay blocks and rod pellets manufactured with bentonite from Milos (Greece) are the elements selected as backfill material for the backfilled drifts. This paper describes an experimental program and the corresponding modeling in order to characterize the hydro-mechanical behavior of pellets. At least, two levels of porosity can be distinguished in pellets: microporosity and macroporosity. In general, the microstructure is associated with the active clay minerals, while the macrostructure accounts for the larger-scale structure of the material. In pellets, this concept can be somewhat different as a pellet arrangement creates a large scale macro pore structure.

The Barcelona Expansive Model is proposed to reproduce the material response through infiltration and oedometer tests. In addition to expansive model parameters, a set of hydraulic laws considering the double structure phenomena is necessary to perform Hydro-Mechanical (HM) analysis. This paper also describes the effect of macro porosity on the intrinsic permeability changes. To illustrate the general objectives of this research, a full scale Thermo-Hydro-Mechanical (THM) calculation has been done to show the capabilities of the approach. Barcelona Basic Model (for clays) and Barcelona Expansive Model (for pellets) have been used in this full scale calculation.

KEY WORDS: Barcelona expansive model, macro and micro-porosity, KBS-3 design, THM calculations, rod pellets, pillow pellets

1. INTRODUCTION

The spent nuclear fuel repository design in Finland follows the KBS-3 design (SKB, 2010). This design has two alternatives: the KBS-3V (Juvankoski et al., 2012) and the KBS-3H (Posiva, 2013). In the KBS-3V alternative, the vertical deposition holes need some clearance for bentonite buffer blocks installation. Therefore, there will be an unavoidable gap between the bedrock and bentonite buffer. The gap filling with pellets both in deposition holes and in tunnel backfill cases has been widely studied (Holt et al., 2013).

The main reason for using pellets in the outer gap, instead of leaving it empty, is to ensure that the density after saturation is sufficiently high for the reference geometry of the blocks and deposition hole. This density should be between 1950 and 2050 kg/m^3 (Juvankoski et al., 2012). In case that pellets were not used, the gaps would have to be narrow to ensure a sufficiently high final density of the buffer. Narrow gaps lead to strict limitations of the acceptable variations of the geometry of the deposition holes and high precision of the installation technique. The pellet filling also prevents falling backfill material into the deposition hole during the backfilling operation of the drift, and may also mitigate the impact of thermally induced spalling in the deposition hole (SKB, 2010).

2. EXPERIMENTAL PROGRAM

Experiments on Pillow Pellets (pellets to be used in buffer) and Rod Pellets (pellets to be used in backfill) are presented in this section. Infiltration tests at constant volume and oedometric tests have been carried out at B+Tech (www.btech.fi) laboratory.

2.1. DESCRITION OF MATERIALS

Pillow pellets were manufactured with MX-80 bentonite. The characterization of the raw material is described in Kiviranta et al., (2016) and Table 1 presents the main properties. The ID material is Be-Wy--BT0027-Pp-R according to Kiviranta et al., (2016).

Figure 1 shows the size of the pellets proposed for filling the space between the buffer blocks and the host rock (Figures 1-A and 1-B). The pillow pellets have a breadth of around 12.0 mm and a thickness of around 5.5 mm. These pellets were manufactured by compaction of the MX-80 clay to small pillow-shaped pieces with a roller compactor (Juvankoski et al., 2012).

Rod pellets were manufactured from Milos bentonite. The characterization of the raw material is also described in Kiviranta et al., (2016) and Kiviranta and Kumpulainen (2011). Table 1 presents the main properties of these two clays. The ID for the material is Be-Mi--NaA-BT0021-Pp-R.

The pellets have a length of 9.4 mm and a diameter of 6.2 mm although the variation of these values is high. The pellets were manufactured by the extrusion method (Keto et al., 2013).

The rod pellets component (Figure 1-C) is used for filling the space between the backfill blocks and the tunnel wall (Figure 1-D) (Keto et al., 2013). The rod pellet material is expected to represent a potentially significant proportion of the tunnel cross-section.

2.2. DESCRIPTION OF TESTS

This section describes the set-up of the tests and the results obtained (Pintado et al., 2013; Kiviranta et al., 2016). As pellet materials have a relatively large pellet (particle) size, the ratio between cell size and particle size might not be optimum. In this regard, the maximum particle size is the limitation of the test set-ups, so the maximum particle size fixes the minimum size of the cell. This limitation may be different as a function of the tests, so (1) in unconfined tests, the diameter should be ten times the maximum diameter of the largest particle (ASTM D2166-06), (2) in oedometer tests, the height should be ten times the maximum particle diameter (ASTM D2435/D2435M-11) and (3) in triaxial tests, the diameter should be six times the maximum particle diameter (ASTM D4767-11). This is important to mention because the size of the pellets is larger than the maximum particle size defined by the ASTM standards. The diameter of the piston in the oedometric test is 50-70 mm (see detailed description below) and pellets have an equivalent diameter in the range of 5 to 7 mm. With these sizes, the contact of the piston or porous stone with the pellet material may be not optimum especially at the beginning of the test. The contact improves as compression and wetting take place and the material tends to homogenize. Water content was measured following the ASTM D2216-10 and the bulk density of the soil specimens following the procedure described in Sartorius density determination kit.

INFILTRATION TESTS

Pellets are in unsaturated conditions when inserted in the deposition holes and are saturated with the blocks as the groundwater flows into the tunnels and deposition holes. The saturation process starts when the water flows in a natural way from the host rock.

Usually, the non-saturated hydraulic conductivity can be measured in porous materials by suction controlled oedometer tests (Romero et al., 1999). However, these tests cannot be performed in bentonites due to their high suction. In this case, for measuring the non-saturated hydraulic conductivity, it is necessary to perform inverse analysis from infiltration tests (Pintado et al., 2002; Villar et al., 2005). Dueck and Nilsson (2010) presented a test where the boundary condition on the inlet water side was high relative humidity control instead of constant water pressure control.

Hoffmann et al., (2007) and Alonso et al., (2011) have carried out investigation on pellets manufactured with FEBEX bentonite. Hoffman (2005) also presents infiltration tests conducted on the same bentonite.

As shown in Figure 2, the infiltration tests involve a column of pellets with initial conditions as given in Table 2. The infiltration cell is made of stainless steel. The inner diameter of the infiltration cell is 50 mm, and the height of the sample is approximately 63 mm. There are two sintered porous frits made of stainless-steel balls with a diameter of 10 μm at the top and bottom of the sample. The pellets were placed directly inside the cells without compaction. The initial dry density was calculated knowing the initial pellets mass and the volume, calculated as the difference between the total volume of the cylinder and the part of the piston inside it. During the tests, a target water pressure was applied at the bottom of the sample by a pressure/volume controller manufactured by GDS (www.gdsinstruments.com). On the top of the sample, the boundary condition was supposed to be a seepage boundary condition. This means that there is not flow of water when the soil is still unsaturated and when it reaches the saturation, the water pressure is fixed in 0 (atmospheric pressure) and there is water flow in liquid phase through the boundary. The real boundary condition is an evaporation but in the conditions of the sample, this evaporation can be considered negligible due the long time necessary for reaching the steady state conditions when the boundary condition is imposed just fixing the relative humidity without forcing air movement through the boundary or through the sample (Pintado et al., 2009). The tests were performed at the laboratory room temperature (approximately 24 °C). The suction of the pellets was measured before the tests with a chilled mirror psychrometer WP-4 (www.decagon.com). The sample volume was kept constant during the test, and the water inlet flow was measured continuously. At the end of the test, the final weigh of the sample was measured. The final volume was also measured with a caliper. The sample was cut into slices with a saw. After cutting the sample, the water content and bulk density were measured. In addition, the suction was measured with the psychrometer.

It can be observed that the dry density is lower near the injection zone which indicates that swelling has taken place. Figure 3 shows the final distribution of dry density (A and B) and water content (C and D)) for pillow and rod pellets at different days. The swelling near the injection zone is possible because other parts of the sample undergo compression. Some level of suction is still measured at the end of the test. This means that the sample is not fully saturated which could be motivated by dismantling of the sample. Dismantling has an associated unloading which may induce some suction due to the swelling developed. The initial and final volume was measured and there were some differences, in some cases, the initial volume was higher and in some cases, lower. The differences were less than 2.5% and were related with the uncertainties in the measurements, especially in the initial volume which was not obtained directly but as difference between different lengths, accumulating the error. It should be also mentioned that the sample may dry out during the dismantling and measuring operations. Figure 4 shows the samples

after the tests. It is possible to see clearly that the pellets structure had not disappeared yet.

OEDOMETER TESTS

The oedometer cells were made of stainless steel. In case of pillow pellets tests, the diameter of the samples is 70 mm and the height 25 mm. The samples for rod pellet tests have a diameter of 50 mm and a height of 36 mm. There are two stainless-steel porous frits at the top and bottom of the sample to facilitate the hydration process. A linear variable differential transformer (LVDT) was used to measure the axial displacements. In addition, a force transducer was placed on the radial direction of the samples to measure the radial stresses.

Figures 5-A and 5-B present the layout of the oedometer test and a picture of the setup in B+Tech laboratories. There is a cell with a hydration facility and a loading arm lever. A weight was placed on the lever to exert axial pressure on the samples.

The pellets were placed directly in the cells. The initial conditions of the samples are given in Table 3. Dry densities were relatively low, 947 kg/m^3 for pillow pellets and 855 kg/m^3 for rod pellets. The degree of saturation was somewhat above 20%, similar for the two samples.

The void ratio versus vertical stress curves for the experimental program and the developed radial stresses due to vertical loading are shown in Figure 6. The main difference between the two curves is the initial void ratio, higher for rod pellets than for pillow pellets, corresponding to the lower dry density. The curves do not show an evident existence of a pre-consolidation pressure as expected since the material was not compacted before compression.

3. MODELING of EXPERIMENTS

The Barcelona Basic Model BBM (Alonso et al., 1990) presents limitations for modeling double structure in clay materials. Therefore, the Barcelona Expansive Model BExM was developed (Gens and Alonso, 1992; Alonso et al., 1999; Sánchez et al., 2005; see Appendix A for brief description) to represent better expansive response of clay materials. The expansive model incorporates two porosities; macro and micro porosity. Originally, microstructure is associated to clay particles and a macrostructure is associated to the macro pores and coarse aggregates. The microstructure behavior has an impact on the macrostructure behavior.

The micro and macro porosities can be studied with Mercury Intrusion Porosimetry (MIP). The evolution of the porosity can be followed during the hydration process in Seiphoori et al., (2014) for MX-80 and it is possible to see clearly the reduction of the macroporosity as the degree of saturation increases. However, in this paper micro and

macro structure concept is applied only to model the behavior of pellets. Actually, the BExM has been applied to simulate the laboratory tests described above which were carried out on pellet materials.

The model is based on the idea that total deformations have two components which are additive but not independent:

$$d\varepsilon_{kl} = d\varepsilon_{kl}^{Macro} + d\varepsilon_{kl}^{micro} \quad (1)$$

where ε_{kl} are the total strains, ε_{kl}^{Macro} the strains in macroporosity and ε_{kl}^{micro} the strains in microporosity. Additional description about the model is included in Appendix A.

In this section, several cases are presented. Numerical simulations of an infiltration and oedometer tests for pellet based material (pillow pellets and rod pellets) have been performed using the BExM. The mechanical and hydraulic parameters used to simulate these tests are given in Table 4 and Table 5. The BExM is combined with an equation for the intrinsic permeability evolution as function of porosity. In the current approach, intrinsic permeability is calculated as a function of the macroporosity. During hydration, pellets expand thus reducing the volume of macropores and a reduction of intrinsic permeability is calculated. The numerical simulations have been performed with CODE_BRIGHT (Olivella et al., 1994, 1996).

3.1. NUMERICAL SIMULATION OF INFILTRATION AND OEDOMETER TEST RESULTS FOR PILLOW PELLETS

The pillow pellets were subjected to 31 days of water infiltration. As it can be seen in Figure 4, macro pores of the sample were almost invisible after hydration. The transition from a pellet discontinuous arrangement to a more homogeneous material, which is visible in Figure 4, is a feature that the BExM model can represent to some extend while BBM does not include.

One of the objectives of this work is to contribute to the development of a conceptual model for the hydration of pellets. An interesting issue on the hydro-mechanical response of pellets is the intrinsic permeability. As indicated above, it is assumed here that intrinsic permeability is a function of macro porosity with the following form:

$$\mathbf{k} = \mathbf{k_0}\exp\left(b(\phi^{Macro} - \phi_0^{Macro})\right) \quad (2)$$

Where $\mathbf{k}_0$ is a reference intrinsic permeability tensor, b is a parameter and ϕ_0^{Macro} is reference macro porosity. During the test, macro porosity decreases due to the swelling of the pellets, and this happens at all points of the sample which is subjected to hydration at constant volume. As intrinsic permeability is considered a function of macro porosity, intrinsic permeability reduces due to macro porosity reduction.

The relative permeability is calculated as follows (Brooks and Corey, 1964).

$$k_{rl} = S_e^m \tag{3}$$

Where m is a parameter and S_e is the effective degree of saturation defined below. This relation has also been used by Gens et al., 2009 in FEBEX bentonite and by Romero et al., 2001 for Boom clay. The value of m was 3, the same value chosen by Pintado and Rautioaho (2013) and Gens et al., 2009.

Water retention curve follows the Van Genuchten model (Van Genuchten, 1980):

$$S_e = \frac{S_r - S_{min}}{S_{max} - S_{min}} = \left(1 + \left(\frac{P_g - P_l}{P_0}\right)^{\frac{1}{1-\lambda}}\right)^{-\lambda} \tag{4}$$

Where P_0, λ, S_{min} and S_{max} are parameters. The liquid flux is calculated following Darcy´s law written in a general form as:

$$\mathbf{q_l} = -\frac{k_{rl}\mathbf{k}}{\mu_l}(\boldsymbol{\nabla} P_l - \rho_l \mathbf{g}) \tag{5}$$

Where $\mathbf{k}$ is intrinsic permeability, k_{rl} is relative permeability, ρ_l is density, μ_l is viscosity, $\boldsymbol{g}$ is gravity vector, and P_l is liquid pressure.

The mechanical and hydraulic parameters are listed in Tables 4 and 5.

The changes in void ratio during the loading-unloading step in the oedometer tests for three set of parameters (κ^{micro}=0.045; κ^{micro}=0.09 and κ^{micro}=0.135) is presented in Figure 7-A. This sensitivity analysis on κ^{micro} has been performed to capture the expected behavior of pellets in infiltration test. The evolution of porosity as a function of time for three set of parameters (κ^{micro}=0.045; κ^{micro}=0.09 and κ^{micro}=0.135) is shown in Figure 7-B. The loading of the sample causes decrease of both macro porosity and total porosity. During compression, micro porosity increases somewhat according to model calculations. This is not surprising as it is defined with respect to the total volume of the sample. During unloading, macro pores are elastically recovered.

Figure 8 shows calculated variables for the infiltration test. It displays the evolution of macro, micro and total porosity for two set of parameters (κ^{micro}=0.045 and κ^{micro}=0.135) close to the top of the sample (Figure 8) and distribution of porosity at the end of the test (35 days).

Figure 9 shows the final profile of dry density (Figure 9-A) and of suction (Figure 9-B) along the sample for two set of parameters (κ^{micro}=0.045 and κ^{micro}=0.135), as a function of the distance from the injection point. The numerical simulation reproduces well the measurements at the end of the test, except for suction near the injection point. The sample was still not completely saturated at the moment of dismantling. It has already been mentioned that it is possible that unloading may have induced a small suction increment or drying out has taken place during the test dismantling and measurement operations.

A sensitivity analysis on κ^{micro} have been performed in oedometer and infiltration tests. Three sets of parameters (κ^{micro}=0.045; κ^{micro}=0.09 and κ^{micro}=0.135) are considered for modelling the oedometer and infiltration tests. With a lower κ^{micro} (0.045) oedometer simulation captures the test results better. A higher κ^{micro} (0.135) produces larger elastic swelling capacity in infiltration test which is consistent with the results of the infiltration tests. The total porosity of the sample remains constant during infiltration for both sets of parameters. However, micro porosity increases because of the expansion of the pellets and there is a consequent reduction of macro porosity. At the end of the test, macro pores have reduced, more significantly for the case that uses a larger parameter for the micro structure swelling (κ^{micro}=0.135).

As indicated above, the parameters for modeling are the same except κ^{micro} which is three times larger in the models for infiltration test than in the model for oedometer test. This larger value seems necessary because for the infiltration test, it is necessary to obtain a significant increase of micro pores (swelling of pellets) and a corresponding reduction of macro pores (occupied by the swollen pellets). In contrast, for the case of the oedometer test simulation, a lower value is required in order to correctly capture the compression and expansion, respectively during loading and unloading.

As it is not possible to model both tests with the same set of parameters, it seems that a modification of the BExM would be necessary in order to separate the elastic deformations of the micro structure by splitting the gradient of p and s into two contributions and hence, having two different values for (κ^{micro}), instead of one. This seems to indicate that the model BExM, in its current form, is more adequate for modeling double structure clays rather than for pellet based materials. In this context, it is likely that pellets would require a triple structure model. The new contribution to deformations can be referred to as deformation at the meso scale.

$$d\varepsilon_{kl} = d\varepsilon_{kl}^{Macro} + d\varepsilon_{kl}^{meso} + d\varepsilon_{kl}^{micro} \tag{6}$$

The idea is that deformation of the pellets is motivated by a combination of the meso structure and a micro structure. The micro structure can be a function of (p+s) because this is related to the deformation of the micro pores of the clay aggregates, which remain practically saturated even when suction develops. The meso structure can be represented by independent terms related to mean net stress and to suction. Finally, macro structure deformations correspond to the deformation associated with pellet reorganization. Development of this kind of model is not straightforward as it requires the incorporation of interaction functions and, at present, there is not enough experimental data. In addition, standard tests such as infiltration and oedometer tests are not able to supply sufficient information for the calibration of the models. The triple structure in pellets has been identified by Hoffman (2005), Hoffmann et al., (2007) and Alonso et al., (2011) in FEBEX pillow pellets.

The evolution of intrinsic permeability and its product by the relative permeability (total permeability is defined as the product of intrinsic and relative permeabilities = $k k_{rl}$) is

depicted in Figure 10-A for two set of paremeters (κ^{micro}=0.045 and κ^{micro}=0.135). The intrinsic permeability is considered as a function of macro porosity as indicated above. It has a lower value at the end of the test because the macro pores close (more significantly, when the microstructure swells more, i.e. when κ^{micro} for infiltration test is used). The model gives small variation of the product of intrinsic permeability and relative permeability although each one undergoes large variations. Intrinsic permeability decreases because macro-pores tend to close while total permeability increases because the material is in a process of saturation. An improved model would require a combination of fluxes through macro pores and micro pores (or even meso pores), at least for the conditions that pellets swell and macro porosity vanishes.

The developed stresses during the infiltration tests two set of parameters (κ^{micro}=0.045 and κ^{micro}=0.135) are shown in Figure 10-B. The stresses developed range from 1.8 to 2.5 MPa depending on the κ^{micro} used.

3.2 NUMERICAL SIMULATION OF OEDOMETER AND INFILTRATION TEST FOR ROD PELLETS

Infiltration and oedometer tests carried out by B+Tech for rod pellets were selected to examine the hydro-mechanical response of the material. Tables 4 and 5 show the values of the parameters used to model the tests.

The experimental and calculated responses of the material in the oedometer test are presented in Figure 11. This plot shows the void ratio versus vertical stress response (Figure 11-A) showing the elastoplastic loading and the elastic unloading. The calculated evolution of total porosity is compared with the measurements (Figure 11-B), and this plot is completed with the predictions using the constitutive model of total porosity, micro porosity and macro porosity. Three set of parameters (κ^{micro}=0.045; κ^{micro}=0.09 and κ^{micro}=0.135) have been used like as in oedometer test for rod pellets. It can be observed that the response of the numerical simulation is better when κ^{micro} is 0.045. The model can successfully reproduce total porosity changes under loading and unloading cycles.

Regarding the infiltration test, Figure 12 shows evolution of macro, micro and total porosity at the top of the sample for two set of parameters (κ^{micro}=0.045 and κ^{micro}=0.135) during the infiltration test. The total porosity of the sample remains nearly constant.

Figure 13 shows the final situation of dry density (A) and suction (B) of the sample in the infiltration test for two set of parameters (κ^{micro}=0.045 and κ^{micro}=0.135) as a function of distance from injection point. The numerical simulation reproduces well the test results for the dry density distribution. At the end of the test, the sample seems to be still unsaturated, since a remaining suction values was measured. However, this may be caused by drying and uncompressing during test dismantling. The suction of top of sample is measured 4 MPa, which is well reproduced by the model.

The evolution of intrinsic permeability and its product by relative permeability are depicted in Figure 14-A. Figure 14 displays curves for two sets of parameters which differ only on the value of κ^{micro} used. The reference value of intrinsic permeability for rod pellets in the infiltration tests is calibrated as 1.4×10^{-18} m^2. Macro porosity is set as 0.307 and total porosity is 0.657. The developed stresses during the infiltration tests are shown in Figure 14-B. The stress developed ranges from 2.8 to 3.5 MPa depending on the κ^{micro} used.

4. THM MODELLING OF VERTICAL DISPOSAL SCHEME INCLUDING SEVERAL PELLET BASED COMPONENTS

An example of use of the expansive model in a disposal scheme is presented in this section. Deposition of spent fuel in vertical boreholes requires using several pellet based components. In a design proposed by POSIVA, pellets are used to fill the gap between the compacted blocks and the host rock, and to backfill parts of the access drift. An axisymmetric geometry has been used to develop a model that allows to get an insight of the behavior of pellet based elements among other aspects of the repository concept.

Nuclear spent fuel produces heat. The conductivity heat flux ($\mathbf{i_c}$) is computed by the Fourier's law:

$$\mathbf{i_c} = -\lambda \boldsymbol{\nabla} T \tag{7}$$

where $\boldsymbol{\nabla} T$ is the gradient of temperature and λ the thermal conductivity calculated as (Villar, 2002):

$$\lambda(S_r) = A_2 + \frac{A_1 - A_2}{1 + \exp[(S_r - S_r^*) / b]} \tag{8}$$

where the parameter S_r^* is the degree of saturation when the thermal conductivity is the average of the dry and saturated thermal conductivities and b is a parameter (Tables 11 and 12).

More information about the solution of the thermal problem can be found in Pintado and Rautioaho (2013) and in Toprak et al., 2013.

Vapour flux $\mathbf{i}_{\mathrm{g}}^{\mathrm{w}}$ close to the canister is computed by Fick's law:

$$\mathbf{i}_{\mathrm{g}}^{\mathrm{w}} = -\left(\tau \phi \rho_g S_g D_m^w \mathbf{I}\right) \boldsymbol{\nabla} \omega_g^w \tag{9}$$

where τ is the tortuosity, ϕ the porosity, ρ_g the density of gas, $S_g = 1 - S_r$, D_m^w the molecular diffusion of vapour (DIT-UPC, 2017) and ω_g^w the mass fraction of vapour in gas. The value chosen for τ in all materials is 0.4 (Pintado and Rautioaho, 2013).

More information about vapour flux can be found in Olivella and Gens (200), Pintado and Rautioaho (2013) and in Toprak et al., 2013 as well. Other works related with the

simulation of a spent nuclear fuel repository can be found in Gens et al., 2009, Chen and Ledesma, 2009, Åkesson et al., 2009 and Åkesson et al., 2010 and Dupray et al., 2011.

4. 1. DESCRIPTION OF VERTICAL DISPOSAL MODEL

Figure 15 describes the vertical disposal scheme including different components. This geometry has been developed according to Keto et al., 2013. Drift backfill has three components, namely: Friedland clay as the main component, rod pellets in contact with the drift wall and a foundation layer made of granules. The buffer material has also two components: discs and rings made of MX-80 bentonite and a vertical layer of pillow pellets in between the bentonite and the host rock. There is an air gap between the canister and the ring blocks. The thickness of this air gap is 10 mm. Material properties are given in Tables 6 to 12.

For pellet based materials, a mean value for κ^{micro} (0.09) has been considered in the disposal scheme modelling. This is motivated by the fact that there was not a single value adequate for both oedometer (0.045) and infiltration tests (0.135). Modification of the BExM equations is far beyond the objectives of this paper.

Figure 15 shows the geometry together with the materials and the mesh. The foundation layer made of granules is 0.4 m thick. Rod pellets, which are in the space between the Friedland clay and the drift host rock wall, form a layer 0.3 m thick.

A rock fracture is considered at the bottom of the buffer. The equivalent thickness of the fracture is 0.08 m. The reason for the relatively large thickness is just to avoid too small elements that may affect the development of the mesh in the vicinity of the fracture (the fracture is represented with volumetric finite elements). Under hydraulic point of view, the thickness is small enough. This fracture is not playing any specific role from a mechanical point of view.

Figure 16 displays initial and boundary conditions: (A) the assumed initial liquid pressures (initial pressure in rock is considered hydrostatic), (B) the total porosity for all components, (C) the microporosity for rod pellets, pillow pellets and granules, (D) the initial hydraulic boundary conditions and (E) the mechanical boundary conditions.

Initially, the excavation process is simulated. On the upper and lower boundaries, hydro-static water pressure is imposed. The vertical boundaries are impervious to liquid flow except the part of the fracture, which has the hydrostatic pressure considering its deep. There is also specific water supply from the rock fracture. The axisymmetric condition of the model only permits to incorporate a somewhat simplified fracture which is assumed horizontal and reaching the borehole at the bottom zone.

The system is confined. With regard to thermal conditions; the upper and lower boundaries have prescribed temperature, vertical boundaries are impervious to heat flow. Heat flux from canister is modelled as volumetric power which decays according to

decaying of spent fuel. The initial power is 410 W/m^3 which corresponds to 1700 W for a single canister, approximately. Detailed information about thermal and coupled THM calculations can be found in Toprak et al., (2013, 2016).

The impervious to liquid and heat boundary condition at the vertical boundaries means that the model represents an infinite set of deposition holes where the liquid and heat flow are not allowed due to the presence of other deposition holes around the simulated deposition hole.

In the model, MX-80 and Friedland clay are modelled with BBM and its parameters are given in Tables 7, 9 and 11. Rod and pillow pellets and granules are simulated with BExM model, and the corresponding parameters are presented in Tables 8, 10 and 12. Hydro-mechanical parameters for rock and THM parameters for air gap are included in Tables 6, 9 and 11.

4.2. RESULTS FOR VERTICAL DISPOSAL MODELLING

Figure 17-A shows temperature evolution for representative points. The maximum temperature is fairly below 90ºC. The effect of air gap can be certainly seen through the Figure. This is evident as temperature at both sides of the gap is different by nearly 10ºC before 2 years but reduces significantly afterwards. The imposed variable temperature on boundaries is also depicted in this figure, this is necessary to account for the relatively close boundaries of the modelled domain. Figure 17-B shows evolution of liquid pressure. It can be seen the de-saturation of the area adjacent to canister in Figure 17-B. The saturation of the system occurs at around 10 years (or somewhat afterwards), according to the represented points. Figure 17-C shows the generation of effective stresses in the buffer and backfill induced by swelling. In the buffer it reaches the value of 7 MPa. As full saturation is reached, swelling stops and the effective stress approach for saturated soils is recovered. At this time, effective stress decreases because the pore pressure development towards hydrostatic conditions. The long term decrease of effective stress after saturation is motivated by the progressive temperature decrease towards ambient conditions.

The vertical displacements at the intersection of buffer and backfill are presented in Figure 17-D. It is observed that the tendency is that the buffer penetrates in the backfill, which is motivated by the relative higher swelling capacity of the buffer with respect to the backfill. Maximum vertical displacements reach a value of 10 cm.

The total porosity and micro porosity calculated evolutions for rod pellets, pillow pellets and granules are depicted in Figure 18. Due to hydration and the corresponding swelling, micro porosity increases. Since total porosity changes only slightly, the increase in micro porosity induces a reduction of the macro porosity.

Figure 19-A depicts the evolution of intrinsic permeability and Figure 19-B shows the evolution of total permeability (total permeability is defined here as the product of

intrinsic permeability and relative permeability). According to the flow model, the first depends on porosity while the second on both, porosity and degree of saturation.

There are not big changes in the intrinsic permeability for MX-80 and Friedland clay, which is not surprising as for these clay materials, the calculated variation of porosity is small (only total porosity is calculated with BBM). Total porosity cannot undergo big variations as the engineered barrier (clay materials) is confined. Modelling with BBM gives only the variation of total porosity, only local expansion and the corresponding compression in other zones may produce total porosity variations.

In contrast, intrinsic permeability of Pillow pellets, Granules and Rod pellets decreases during saturation process. This is motivated by the decrease of macroporosity caused by the microporosity increase, while total porosity changes are moderate. As indicated, total permeability is the product of intrinsic permeability and relative permeability. For pellet based materials, intrinsic permeability is calculated from macroporosity assuming that water in micropores does not contribute to flow significantly. Finally, although intrinsic permeability decreases, total permeability increases during saturation process and tends to reach the steady state condition.

5. CONCLUSIONS

In order to represent the hydro-mechanical behavior of pellets, a model with two pore structure has been considered. The macrostructural level has a role to play in the global arrangements of clay aggregates while the microstructural level controls the swelling and shrinkage. The intrinsic permeability is governed by macro porosity in the model presented. The model has exhibited good performance with the experimental results of both pillow pellets and rod pellets.

The process of calibration has shown that it is difficult to represent the deformation of the microstructure using a single term proportional to variations of (p+s). Actually, it has been found that the parameter for this term requires a larger value for the modeling of the infiltration tests as compared with the modeling of the oedometer tests. The same drawback was found for both the pillow pellets and the rod pellets.

Improvements of the BExM coupled to permeability equation for pellets seem necessary. Essentially it has been found that the microstructural deformation cannot be calculated using the variable (p+s). So it was necessary to use a different coefficient κ^{micro} depending on whether the test simulated was the infiltration test or the oedometer test. A compromise value for κ^{micro} has been considered to calculate the behavior of pellets based materials in the disposal scheme.

On the other hand, it seems that the intrinsic permeability being solely a function of macro porosity is not sufficiently adequate because macro porosity can reduce and practically disappear under conditions of high swelling of pellets. This phenomenon can be seen in Seiphoori et al., (2014) for MX-80 samples compacted at relatively high density (1800

kg/m^3) although in FEBEX bentonite pellets, it is possible to see two and even three levels of porosity (Hoffmann, 2005).

A full scale THM calculation has been performed to evaluate model performance. The progress of hydration, development of swelling pressure, displacements and effects of heating were the main attention of THM calculations. Material parameters used in this calculation are determined from an extensive programme of laboratory tests (only tests for pellet based materials are described and modelled in this paper).

Acknowledgements

This work was financed in part by B+Tech Oy (Finland) under a POSIVA Oy project. The authors thank Noora Kanerva, Nora Akhanoba, Oyinloye Femi Adesola and Mamunul Hassan for collaboration in the experimental work. Authors also thank to Kari Koskinen and Mika Niskanen for the management of the project.

Appendix

Barcelona Expansive Model (BExM) is an extension of Barcelona Basic Model (BBM) to reproduce fundamental features of expansive soils that have double structure. Microstructural behavior controls the swelling and shrinkage of aggregates while macrostructure behavior describing the arrangement of the aggregates.

As shown in Figure A1 BExM includes irreversible deformation induced by the swelling and shrinkage of the aggregates. A brief description of the model is included in this appendix.

Total strain is calculated as the sum of Macro and micro deformations:

$$d\varepsilon_{kl} = d\varepsilon_{kl}^{Macro} + d\varepsilon_{kl}^{micro} \tag{A1}$$

These deformations are calculated as:

$$\begin{aligned} d\varepsilon_{kl}^{Macro} &= C_{ijkl}^{Macro} d\sigma_{ij} + \delta_{kl} \frac{ds}{3K_s^{Macro}} + d\varepsilon_{kl}^{LC} + d\varepsilon_{kl}^{SD} + d\varepsilon_{kl}^{SI} \\ d\varepsilon_{kl}^{micro} &= C_{ijkl}^{micro} d\sigma_{ij} + \delta_{kl} \frac{ds}{3K^{micro}} \end{aligned} \tag{A2}$$

Where C_{ijkl}^{Macro} is the mechanical elastic compliance matrix at macro level (inverse of stiffness matrix); C_{ijkl}^{micro} is the mechanical elastic compliance matrix at micro level; K_s^{Macro} is the bulk modulus against suction changes at the macro level; K_s^{micro} is the bulk modulus against suction changes at the micro level; $d\varepsilon_{kl}^{LC}$ are the plastic strains at the macro level when the LC (loading-collapse curve) is activated; $d\varepsilon_{kl}^{SD}$ and $d\varepsilon_{kl}^{SI}$ are the macro plastic strains if the SD (suction-decrease curve) and SI (suction-increase curve) are activated, respectively.

Suction and stress changes induce deformations at the macro and micro level according to the following nonlinear coefficients:

$$K^{Macro} = \frac{\left(1+e^{M}\right)p}{\kappa^{Macro}} \qquad K_s^{Macro} = \frac{\left(1+e^{M}\right)(s+p_{atm})}{\kappa_s^{Macro}} \qquad K^{micro} = \frac{\left(1+e^{m}\right)(p+s)}{\kappa^{micro}} \tag{A3}$$

The increment of volumetric macrostructural plastic deformation due to microstructural swelling or shrinkage is calculated from microstructural deformations using interaction functions. This may happen either when the SD (suction decrease) or the SI (suction increase) curves are activated. The interaction function is defined in the following equation:

$$d\varepsilon_{vM}^{p} = f d\varepsilon_{vm} \tag{A4}$$

And has the following form:

$$f^{SI} = f_{SI0} + f_{SI1}\left(\frac{p}{p_0}\right)^{n_{SI}} \qquad f^{SD} = f_{SD0} + f_{SD1}\left(1-\frac{p}{p_0}\right)^{n_{SD}} \tag{A5}$$

The yield curves SD and SI are described as:

$$F^{SD} = \gamma^{SD} - p - s \qquad F^{SI} = p + s - \gamma^{SI} \tag{A6}$$

And depend on the volumetric deformations via the following hardening equations:

$$d\gamma^{SD} = \frac{K^{micro}}{f^{SD}} d\varepsilon_{vol}^{SD} + \frac{K^{micro}}{f^{SI}} d\varepsilon_{vol}^{SI} \qquad d\gamma^{SI} = \frac{K^{micro}}{f^{SD}} d\varepsilon_{vol}^{SD} + \frac{K^{micro}}{f^{SI}} d\varepsilon_{vol}^{SI} \tag{A7}$$

Finally, the model uses the standard BBM description for the plastic deformations of the macrostructure level:

$$p_0 = p_c\left(\frac{p_0^*}{p_c}\right)^{\frac{\lambda(0)-\kappa^{Macro}}{\lambda(s)-\kappa^{Macro}}} \quad \text{with} \quad \lambda(s) = \lambda(0)\left[(1-r)e^{-\beta s} + r\right] \tag{A8}$$

$$\frac{dp_0^*}{p_0^*} = \frac{(1+e^{Macro})}{\lambda - \kappa}\left(d\varepsilon_{vol}^{LC} + d\varepsilon_{vol}^{SD} + d\varepsilon_{vol}^{SI}\right) \tag{A9}$$

It can be seen that hardening is a function of the volumetric strains caused by SD, SI and LC yield curves. Details about this model can be found in Alonso et al (1999).

References

Alonso, E., Gens, A., Josa, A. 1990. A constitutive model for partially saturated soils. Géotechnique 40(3): 405-430.

Alonso, E.E., Romero, E., Hoffmann, C. 2011. Hydromechanical behaviour of compacted granular expansive mixtures: experimental and constitutive study. Géotechnique 61(4): 329-344.

Alonso, E. E., Vaunat, J., Gens, A. 1999. Modelling the mechanical behaviour of expansive clays. Engineering Geology 54(1): 173–183.ASTM D2166-06. Standard Test Method for Unconfined Compressive Strength of Cohesive Soil.

ASTM D2166-06. Standard Test Method for Unconfined Compressive Strength of Cohesive Soil.

ASTM D2216-10. Standard Test Methods for Laboratory Determination of Water (Moisture) Content of Soil and Rock by Mass.

ASTM D2435/D2435M-11. Standard Test Methods for One-Dimensional Consolidation Properties of Soils Using Incremental Loading.

ASTM D4767-11. Standard Test method for Consolidated Undrained Triaxial Compression Test for Cohesive soils.

Brooks, R.H., Corey, A.T. (1964). Hydraulic Properties of Porous Media. Hydrologic Paper 3, Colorado State University, Fort Collins, USA.

Chen, G. J., Ledesma, A. 2009. Coupled thermohydromechanical modeling of the full-scale in situ test "Prototype Repository". Journal of Geotechnical and Geoenvironmental Engineering 135(1): 121-132.

DIT-UPC. 2017. CODE_BRIGHT User's guide. Departament d'enginyeria del terreny, cartográfica i geofísica. Universitat Politècnica de Catalunya, Barcelona. Spain.

Dueck, A., Nilsson, U. (2010). Thermo-hydro-mechanical properties of MX-80. Results from advanced laboratory tests. SKB Report TR-10-55. Stockholm, Sweden.

Dupray, F., François, B., Laloui, L. 2011. Analysis of the FEBEX multi-barrier system including thermoplasticity of unsaturated bentonite. International Journal for Numerical and Analytical Methods in Geomechanics.

Gens, A., Alonso, E.E., 1992. A framework for the behaviour ical behaviour of unsaturated Boom clay: an experimental of unsaturated expansive clays. Canadian Geotechnical Jorunal 29(6): 1013-1032.

Gens, A., Sánchez, M., Guimaraes, L. do. N, Alonso, E.E., Lloret, A., Olivella, S., Villar, M.V., Huertas, F. (2009). A full-scale in situ heating test for high-level nuclear waste disposal: observations, analysis and interpretation. Géotechnique, 59(4): 377-399.

Johannesson, L-E, Nilsson, U. 2006. Deep repository – engineered barrier systems. Geotechnical behaviour of candidate backfill materials. Laboratory tests and calculations for determining performance of the backfill. SKB R-06-73. Swedish Nuclear Fuel and Waste Management Company (SKB), Stockholm, Sweden.

Johnsson, A., Sandén, T. 2013. System design of backfill. Pellet optimization. SKB report R-13-47. Stockholm, Sweden.

Hoffmann, C. 2005. Caracterización hidromecánica de mezclas de pellets de bentonite. Estudio experimental y constitutivo. PhD dissertation. Technical University of Catalonia. Spain.

Hoffmann, C., Alonso, E.E., Romero, E. 2007. Hydro-mechanical behaviour of bentonite pellet mixtures. Physics and Chemistry of the Earth 32: 832-849.

Holt, E., Loija, M., Fortino, S., Marjaavara, P. 2014. Experimental studies of buffer gap design with artificial wetting. Posiva Working Report 2013-52. Eurajoki, Finland.

Juvankoski, M., Ikonen, K., Jalonen, T. 2012. Buffer production line 2012. Desgin, production and initial state of the buffer. Posiva report 2012-17. Eurajoki. Finland.

Karnland O., Olsson S., Nilsson U. 2006. Mineralogy and sealing properties of various bentonites and smectite-rich clay materials. SKB TR-06-30. Swedish Nuclear Fuel and Waste Management Company (SKB), Stockholm, Sweden.

Keto, P. (editor), Hassan, M, Karttunen, P., Kiviranta, L., Kumpulainen, S., Korkiala-Tanttu, L., Koskinen, V., Jalonen, T., Koho, P., Sievänen, U. 2013. Backfill Production Line 2012. Design, production and initial state of deposition tunnel backfill and plug. Posiva Report 2012-18. Eurajoki, Finland.

Kiviranta, L, Kumpulainen, S., Pintado, X., Karttunen, P., Schatz, T. 2017. Characterization of bentonite and clay materials 2012-2015. Posiva working report 2016-05. Eurajoki. Finland.

Kiviranta, L., Kumpulainen, S. 2011. Quality Control and Characterization of Bentonite Materials. Posiva Working report 2011-84. Eurajoki, Finland.

Kumpulainen S., Kiviranta L. 2010. Mineralogical and chemical characterization of various bentonite and smectite-rich clay materials. Posiva WR 2010-52. Posiva Oy, Olkiluoto, Finland.

Kiviranta, L., Kumpulainen, S., Pintado, X., Karttunen, P. Schatz, T. (2016). Characterization of bentonite and clay materials 2012-2015. Posiva Working report 2016-05. Eurajoki. Finland.

Martino, J., Dixon, D. 2006 Placement and formulation studies on potential light backfill and gap fill materials for use in repository sealing. Report No. 06819-REP-01300-10011-R00. Ontario Power Generation, Nuclear Waste Management Division, Canada.

Marjavaara, P., Holt, H., Sjoblom, V. 2013. Costumized Bentonite Pellets: Manufacturing, Performance and Gap Filling Properties. Posiva Working Report 2012-62. Eurajoki, Finland.

Martikainen, J., Schatz, T. 2011. Laboratory tests to determine the effect of Olkiluoto bounding brine water on buffer performance. Posiva working report 2011-68. Eurajoki. Finland.

Olivella, S., Carrera, J., Gens, A., Alonso, E.E. 1994. Non-isothermal multiphase flow of brine and gas thorough saline media. Transport in Porous Media, 15(3): 271–293.

Olivella, S., Gens, A., Carrera, J., Alonso, E.E. 1996. Numerical formulation for a simulator (CODE-BRIGHT) for the coupled analysis of saline media. Eng. Comput., 1: 87– 112.

Olivella, S., Gens, A. 2000. Vapour transport in low permeability unsaturated soils with capillary effects. Transport in Porous Media, 40:219-241.

Pintado, X., Ledesma, A., Lloret, A. 2002. Backanalysis of thermohydraulic bentonite properties from laboratory tests. Engineering Geology 64: 91-115.

Pintado, X., Lloret, A., Romero, E. 2009. Assessment of the use of the vapour equilibrium technique in controlled-suction tests. Canadian Geotechnical Journal 46: 411-423.

Pintado, X., Rautioaho, E. 2013. Thermo-Hydraulic Modelling of Buffer and Backfill. Posiva Report 2012-48. Eurajoki. Finland.

Pintado, X., Hassan, Md, Martikainen, J. 2013. Thermo-hydro-mechanical tests of buffer Material. Posiva Working Report 2012-49. Eurajoki, Finland.

Posiva, 2013. KBS-3H Complementary Studies, 2008-2010. Posiva Report 2013-3. Eurajoki, Finland.

Pintado, X., Kristensson, O., Malmberg, D., Åkesson, M., Olivella, S., Puig, I. 2017. TH and THM modelling of a KBS-3H deposition drift. Posiva working report 2016-25. Eurajoki. Finland.

Romero, E., Gens, A., Lloret, A. 1999. Water permeability, water retention and microstructure of unsaturated compacted Boom clay. Engineering Geology 54(1-2): 117-127.

Romero, E., Gens, A., Lloret, A. 2001. Temperature effects on the hydraulic behaviour of an unsaturated clay. Geotechnical and Geological Engineering 19: 311-332.

Schatz, T., Martikainen, J. 2012. Laboratory tests and analyses on potential Olkiluoto backfill materials. Posiva working report 2012-74. Eurajoki. Finland.

Sánchez, M., Gens, A., Guimaraes, L do N., Olivella, S. 2005. A double structure generalized plasticity model for expansive materials. International Journal for Numerical and Analytical Methods in Geomechanics. 29(8): 751-787.

Sandén, T., Börgesson, L., Dueck, A., Goudarzi, R., Lönnqvist, M. 2008. Deep repository - engineered barrier system. Erosion and sealing processes in tunnel backfill materials investigated in laboratory. SKB R-08-135. Swedish Nuclear Fuel and Waste Management Company (SKB), Stockholm, Sweden.

Sartorius YDK 01, YDK 01-0D, YDK 01 LP. Density determination kit. User's manual.

Seiphoori, A., Ferrari, A., Laloui, L. 2014. Water retention behaviour and microstructural evolution of MX-80 bentonite during wetting and drying cycles. Géotechnique 64(9): 721-734.

SKB, 2010. Design, production and initial state of the buffer. SKB report TR-10-15. Stockholm. Sweden.

Tang, A.-M., Cui, Y.-J. (2005). Controlling suction by the vapour equilibrium technique at different temperatures and its application in determining the water retention properties of MX80 clay. Canadian Geotechnical Journal (42): 287-296.

Toprak, E., Mokni, N., Olivella, S. & Pintado, X. 2013. Thermo-Hydro-Mechanical Modelling of Buffer, Synthesis Report. Posiva Report 2012-47. Posiva, Eurajoki, Finland.

Toprak, Olivella, S. & Pintado, X. 2016. Coupled THM modelling of engineered barriers for the final disposal of spent nuclear fuel isolation. Radioactive Waste Confinement: Clays in Natural and Engineered Barriers. Geological Society, London, Special Publications

Van Genuchten, R. (1980). A closed-form equation for predicting the hydraulic conductivity of unsaturated soils. Soil Science Society American Journal, 44: 892-898.

Villar, M.V. (2002). Thermo-hydro-mechanical characterisation of a bentonite from Cabo de Gata. A study applied to the use of bentonite as sealing material in high level radioactive waste repositories. Publicación Técnica ENRESA 01/2002. 258 pp. Madrid.

Villar, M.V., Romero, E., Lloret, A. 2005. Thermo-mechanical and geotechnical effects on the permeability of high-density clays. In: Advances in understanding engineered clay barriers. Balkema Publ., Leiden, ISBN: 04-1536-544-9: 177-191.Åkesson, M., Börgesson, B., Kristensson, O. (2010). Sr-Site Data report. SKB Technical report TR-10-44. Stockholm, Sweden.

Åkesson, M., Jacinto, A-C, Gatabin, C., Sánchez, M., Ledesma, A. 2009. Bentonite THM behaviour at high temperatures: experimental and numerical analysis. Geotechnique 59(4): 307-318.

Åkesson, M., Börgesson, B., Kristensson, O. 2010. Sr-Site Data report. SKB Technical report TR-10-44. Stockholm, Sweden.

Table 1. Characterization results on the bentonites

Material	Smectite content (%)	Ex. Ca (%)	Ex. Na (%)	CEC (eq/kg)	Swelling index (ml/2g)	Limit liquid (%)	Grain density (kg/m^3)
MX-80 Clay (Pillow Pellets)	82	18	71	0.86	27.8	578	2806
Milos Clay (Rod Pellets)	69.1	5	87	0.89	27	560	2837

CEC: Cation exchange capacity

Table 2. Material properties and test specifications for infiltration tests

Material	Test ID	Initial Conditions			Test Duration (Days)
		Dry density (kg/m^3)	Initial water content (%)	Initial degree of saturation (%)	
Pillow pellet	141219a	891	16.8	22	31
Rod pellets	131030c	951	18.5	27	15

Table 3. Material properties and test specifications for oedometer tests

Material and its ID	Test ID	Initial Conditions		
		Initial dry density (kg/m^3)	Initial water content (%)	Final dry density (kg/m^3)
Pillow pellet	131118a	947	16.0	1076
Rod pellets	140912b	855	14.4	1242

Table 4. Mechanical parameters used in the numerical simulations

Parameter	Pillow pellets		Rod pellets	
	Oedometer	Infiltration	Oedometer	Infiltration
κ^{Macro} (-)	0.045	0.045	0.045	0.045
κ^{micro} (-)	0.045	0.045[a], 0.3[b] (*)	0.045	0.045[a], 0.4[b] (*)
κ_s^{Macro} (-)	0.01	0.01	0.01	0.01
ν^M (-)	0.3	0.3	0.3	0.3
f_{sd0} (-)	-0.1	-0.1	-0.1	-0.1
f_{sd1} (-)	1.1	1.1	1.1	1.1
n_{sd} (-)	2	2	2	2
f_{si0} (-)	-0.1	-0.1	-0.1	-0.1
f_{sd1} (-)	1.1	1.1	1.1	1.1
n_{si} (-)	0.5	0.5	0.5	0.5
M (-)	1	1	1	1
r (-)	0.8	0.8	0.8	0.8
β (MPa^{-1})	0.0001	0.0001	0.0001	0.0001
p_c (MPa)	0.1	0.1	0.1	0.1
P_{to} (MPa)	0.01	0.01	0.01	0.01
$\lambda(0)$ (-)	0.19	0.19	0.3	0.3
P_0^* (MPa)	2	2	4	4

(*) Two different values are used to model the infiltration test. Depending on the value used, set “a” or set “b” is referred in the text.

Table 5. Hydraulic parameters for pellet based materials (infiltration and oedometer test modelling)

Equation	Parameter	Pellets buffer-rock gap (Pillow)	Pellets backfill-buffer transition (Granules)	Pellets backfill-rock transition (Rod)
Van Genuchten retention curve	P (MPa)	5 (1)	12 (1)	7 (3)
	λ (-)	0.34 (1)	0.4 (1)	0.4 (3)
	a (-) in $P(\phi)$	-	-	-
	b (-)in $\lambda(\phi)$	-	-	-
	ϕ_o	-	-	-
Darcy flux	k (m^2)	$5x10^{-19}$	$1.5\ x10^{-19}$ (2)	$1.4x10^{-18}$
	b (-) in $k(\phi)$	10	10 (2)	10
	ϕ_o	0.319	0.302 (2)	0.35

(1) Kiviranta et al. 2016

(2) Calculated from hydraulic conductivity tests presented in Karnald et al. 2006, Martikainen and Schatz, 2011

(3) Calculated from water retention curve tests presented in Kiviranta et al. 2016

Table 6. Mechanical parameters for air gap element, rock and canister (Toprak et al. 2016)

Parameter	Rock	Canister	Parameters	Gap Element
E (MPa)	63000	21000	E_c (MPa)	100
ν	0.25	0.3	ν	0.3
α ($^oC^{-1}$), linear	$0.85x10^{-5}$	10^{-5}	α ($^oC^{-1}$), linear	-
			E_o (MPa)	1
			Strain limit	0.95

Table 7. BBM Parameters for Buffer and Backfill blocks (Toprak et al. 2016).

Parameter	Symbol	Buffer	Backfill
Poisson ratio (-)	ν	0.3	0.3
Minimum bulk module (MPa)	K_{min}	10	10
Reference mean stress (MPa)	p_{ref}	0.01	0.01
Parameters for elastic volumetric compressibility against mean net stress change (-)	κ_{i0}	0.09	0.05
Parameters for elastic volumetric compressibility against suction change (-)	κ_{s0}	0.09	0.05
Parameter for elastic thermal strain ($^oC^{-1}$)	α	$9x10^{-4}$	$9x10^{-4}$
Slope of void ratio – mean net stress curve at zero suction (-)	$\lambda(0)$	0.25	0.18
Parameters for the slope void ratio – mean net stress at variable suction (- , MPa^{-1})	r	0.8	0.8
	β	0.02	0.02
Reference pressure for the P_0 function (MPa)	p^c	0.1	0.1
Pre-consolidation mean stress for saturated soil (MPa)	P_o*	2	2
Critical state line (-)	M	1.07	1.07

Table 8. BExM Parameters for Pellet based materials (vertical disposal modelling)

Parameter	Pellets buffer-rock gap (Pillow)	Pellets backfill-buffer transition (Granules)	Pellets backfill-rock transition (Rod)
κ^{Macro} (MPa)	0.045	0.045	0.045
κ^{micro} (MPa)	0.09	0.09	0.09
κ_s^{micro} (MPa)	0.01	0.01	0.01
$K_{\min}^{Macro}$ (MPa)	10	10	10
$K_{\min}^{micro}$ (MPa)	0.001	0.001	0.001
ν^M (-)	0.3	0.3	0.3
f_{sd0} (-)	-0.1	-0.1	-0.1
f_{sd1} (-)	1.1	1.1	1.1
n_{sd} (-)	2	2	2
f_{si0} (-)	-0.1	-0.1	-0.1
f_{sd1} (-)	1.1	1.1	1.1
n_{si} (-)	0.5	0.5	0.5
M (-)	1	1	1
r (-)	0.8	0.8	0.8
β (MPa^{-1})	0.0001	0.0001	0.0001
p_c (MPa)	0.1	0.1	0.1
P_{to} (MPa)	0.01	0.01	0.01
$\lambda(0)$ (-)	0.19	0.3	0.3

Table 9. Hydraulic parameters for rock, buffer, backfill and gap (vertical disposal modelling)

Equation	Parameter	Rock	Buffer	Backfill	Gap element
Van Genuchten retention curve	P (MPa)	1.5 (1)	27 (2)	4.5 (3)	0.001
	λ (-)	0.3 (1)	0.45 (2)	0.25 (3)	0.5
	a (-) in $P(\phi)$	-	11 (2)	22 (3)	15
	b (-)in $\lambda(\phi)$	-	4 (2)	8 (3)	-
	ϕ_0	-	0.4245 (2)	0.393 (3)	0.8
Darcy flux	k (m^2)	$1.52x10^{-19}$ (1) (Fracture: $1.52x10^{-16}$)	$5.6x10^{-21}$ (1)	$7.6x10^{-20}$ (4)	10^{-16}
	b (-) in $k(\phi)$	-	15 (1)	16 (4)	15
	ϕ_0	-	0.438 (1)	0.36 (4)	0.8

(1) Pintado and Rautioaho, 2013

(2) Pintado et al. 2017

(3) Kiviranta et al. 2016

(4) Calculated from oedometer test results for DI water presented in Kiviranta et al. 2016 and hydraulic conductivity tests presented in Karnland et al. 2006, Johannesson and Nilson, 2006, Sandén et al. 2008 and Schatz and Martikainen, 2011

Table 10. Hydraulic parameters for pellet based materials (vertical disposal modelling)

Equation	Parameter	Pellets buffer-rock gap (Pillow)	Pellets backfill-buffer transition (Granules)	Pellets backfill-rock transition (Rod)
Van Genuchten retention curve	P (MPa)	5 (1)	12 (1)	7 (3)
	λ (-)	0.34 (1)	0.4 (1)	0.4 (3)
	a (-) in $P(\phi)$	-	-	-
	b (-)in $\lambda(\phi)$	-	-	-
	ϕ_0	-	-	-
Darcy flux	k (m^2)	$5x10^{-19}$	$1.5\ x10^{-19}$ (2)	$1.4x10^{-18}$
	b (-) in $k(\phi)$	10	10 (2)	10
	ϕ_0	0.319	0.302 (2)	0.35

(4) Kiviranta et al. 2016

(5) Calculated from hydraulic conductivity tests presented in Karnald et al. 2006, Martikainen and Schatz, 2011

(6) Calculated from water retention curve tests presented in Kiviranta et al. 2016

Table 11. Thermal parameters for rock, canister, buffer, backfill and gap (vertical disposal modelling, Pintado et al. 2017)

Parameter	Rock	Canister	Buffer	Backfill	Gap element
ρ_s (kg/m^3)	2743	8930	2780	2780	-
c_s (J/kg·K)	764	390	830	800	-
$A_1 \approx \lambda_{dry}$ (W/m·K)	2.82(1)	390	0.2	0.2	0.045
$A_2 \approx \lambda_{sat}$ (W/m·K)	2.82(1)	390	1.4	1.4	0.6
b in $\lambda(S_r)$	-	-	-0.15	-0.15	-
S_r* in $\lambda(S_r)$	-	-	0.5	0.5	-
$\phi_{initial}$ (-)	0.005	0.01	0.37/0.388	0.27	0.8

(1) Rock thermal conductivity is constant

Table 12. Thermal parameters for pellet based materials (vertical disposal modelling, Pintado et al. 2017).

Parameter	Pellets buffer-rock gap (Pillow)	Pellets backfill-buffer transition (Granules)	Pellets backfill-rock transition
ρ_s (kg/m^3)	2780	2780	2780
c_s (J/kg·K)	830	830	830
$A_1 \approx \lambda_{dry}$ (W/(m·K))	0.16	0.2	0.16
$A_2 \approx \lambda_{sat}$ (W/(m·K))	0.63	0.63	0.63
b in $\lambda(S_r)$ (-)	-0.15	-0.15	-0.15
S_r* in $\lambda(S_r)$ (-)	0.6	0.5	0.6
$\phi_{initial}$ (-)	0.669	0.552	0.7

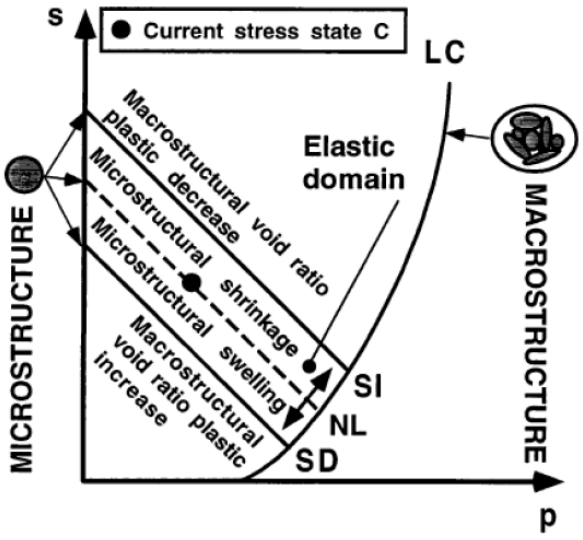

Figure A1. BExM assumptions on the behavior of macro and micro structure

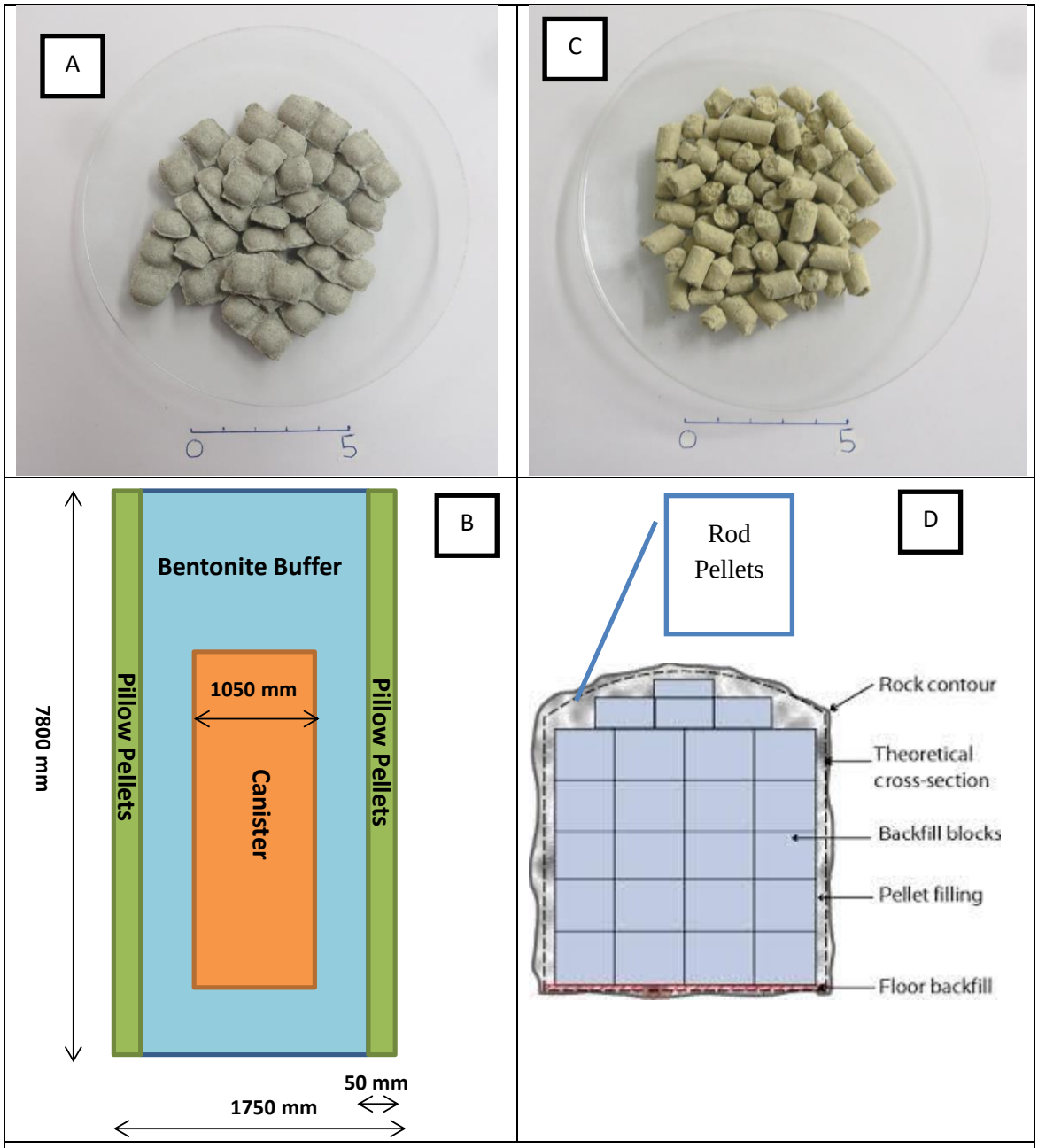

Figure 1. Examples of bentonite pellets used in repository sealing studies and their location. Pillow pellets (A) and their location (B); Rod pellets (C), the batch is different but basically, the pellets were the same, and their location (D). Dimensions in (A) and (B) in cm.

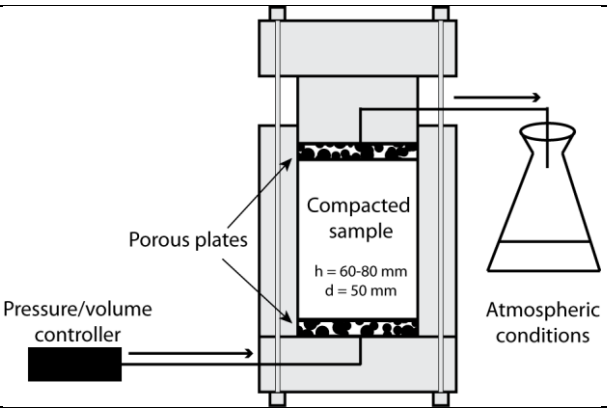

Figure 2. Diagram of the infiltration test setup.

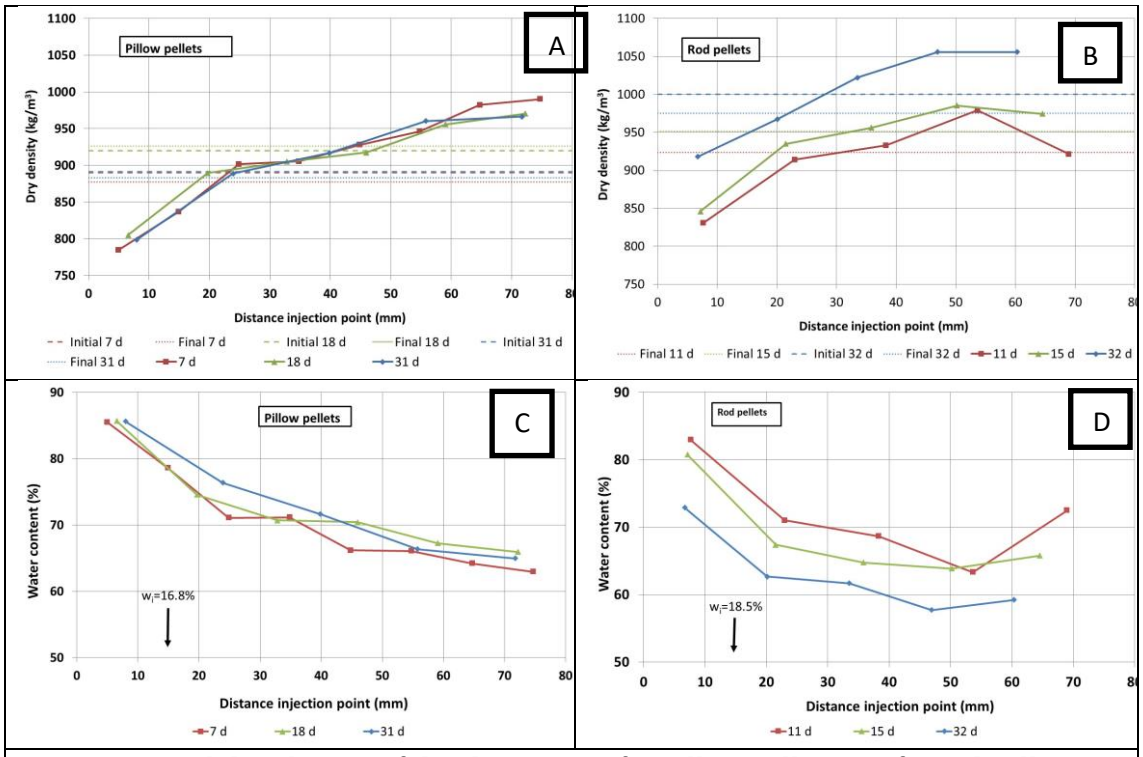

Figure 3. Final distribution of dry density (A) for pillow pellets (B) for rod pellets and water content (C) for pillow pellets and (D) for rod pellets in the infiltration tests. (Experimental results). The initial dry density and the final average dry density are indicated with dashed black lines.

Figure 4. Sample of pillow pellet (left) and rod pellets (right) at the end of the infiltration test. Diameter of the samples: 50 mm.

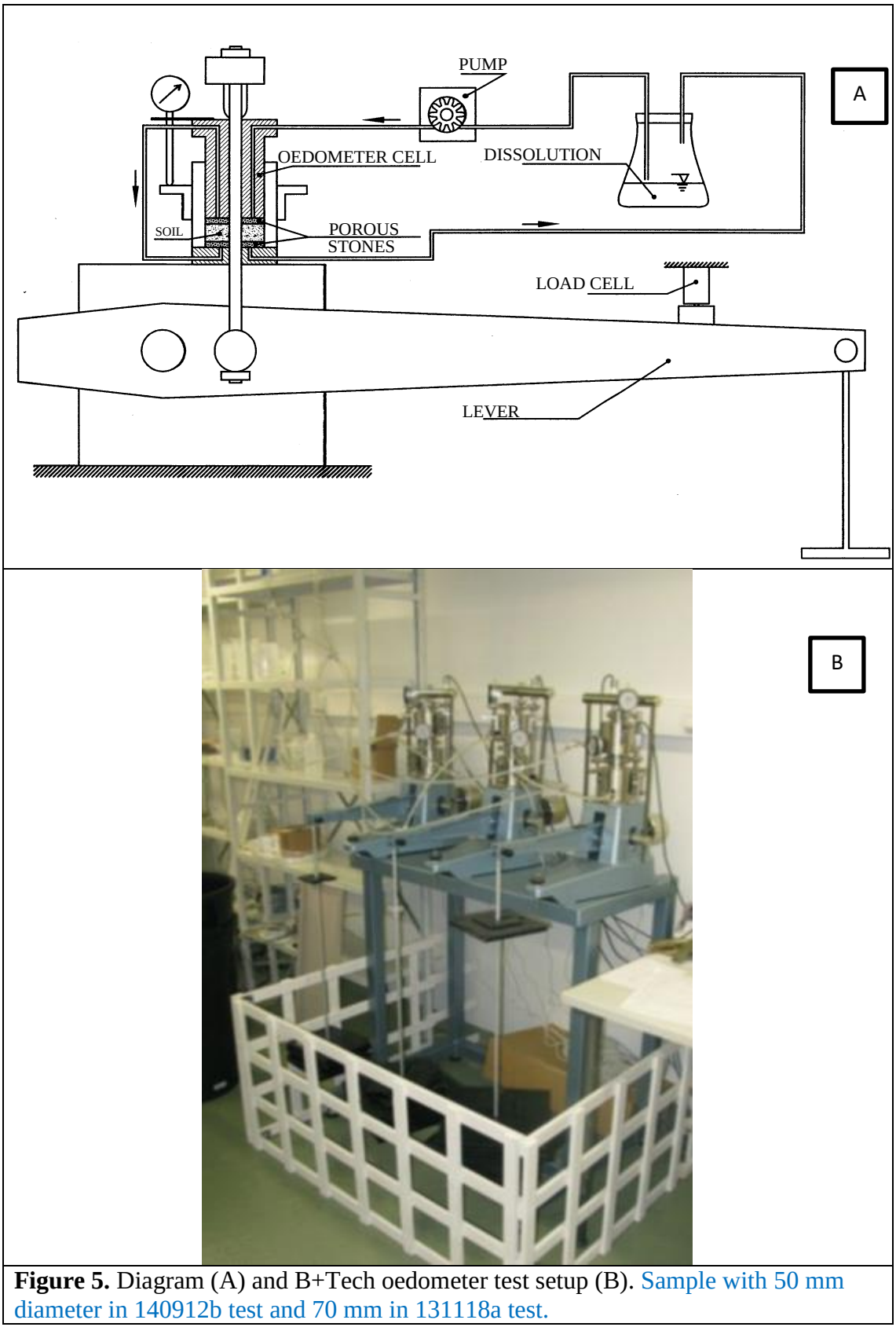

Figure 5. Diagram (A) and B+Tech oedometer test setup (B). Sample with 50 mm diameter in 140912b test and 70 mm in 131118a test.

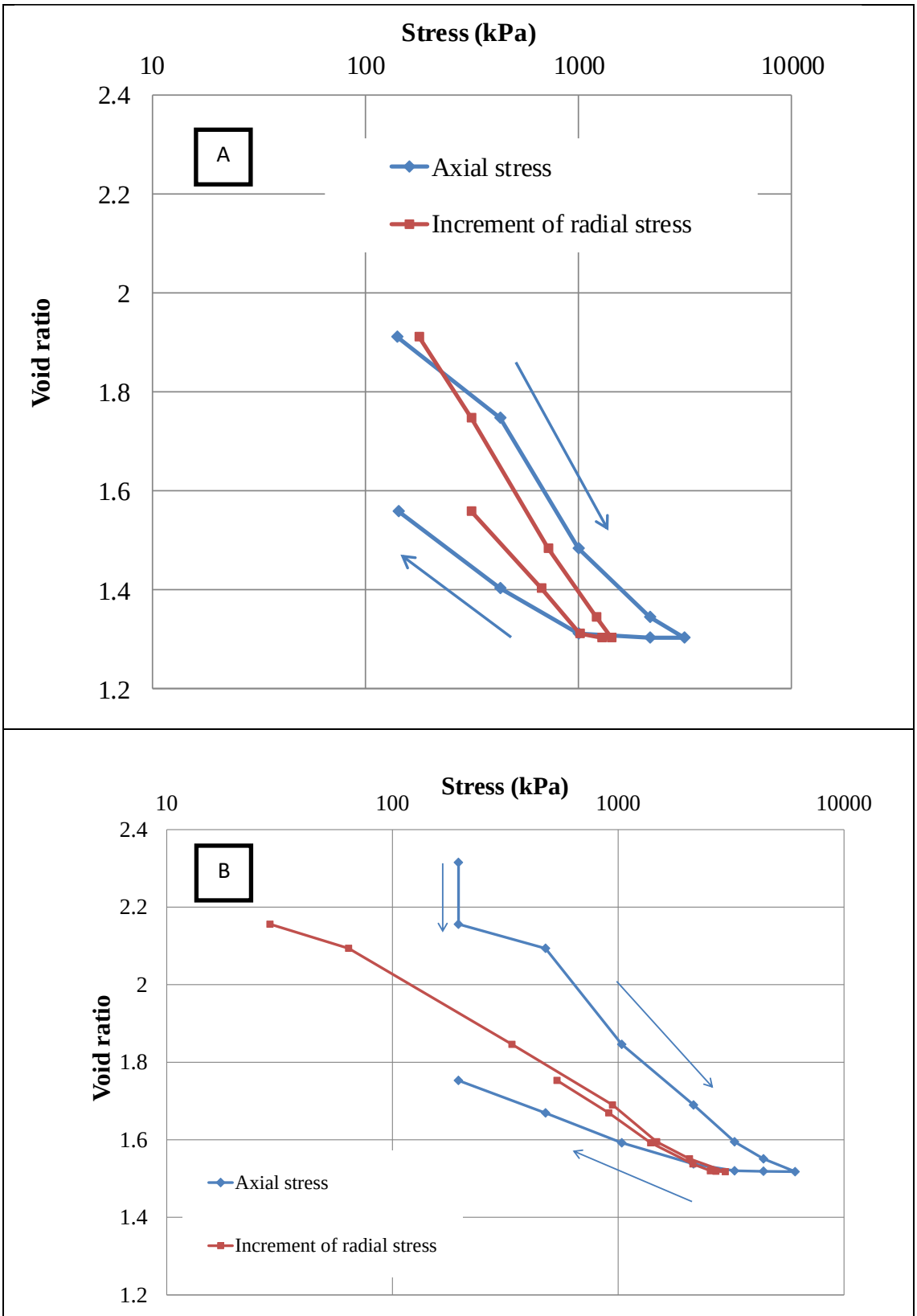

Figure 6. Changes in void ratio as a function of axial stress in oedometer tests for pillow pellets (A) and rod pellets (B) (Experimental results).

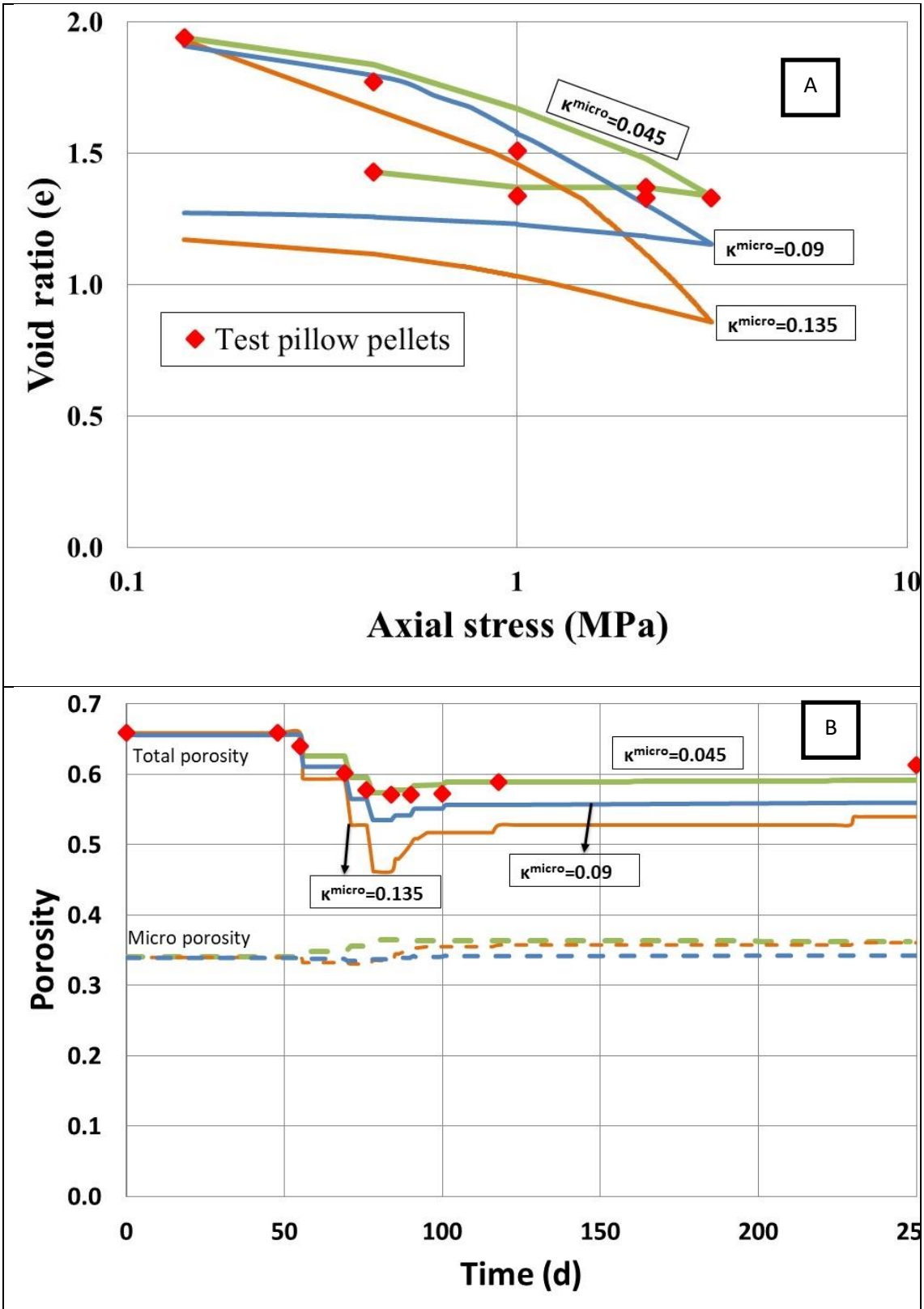

Figure 7. Void ratio vs. axial stress (A) and porosity vs. time (B) in the oedometer test for pillow pellets, three set of parameters (κ^{micro}=0.045; κ^{micro}=0.09 and κ^{micro}=0.135) are subjected to sensitivity analysis (experimental and model results).

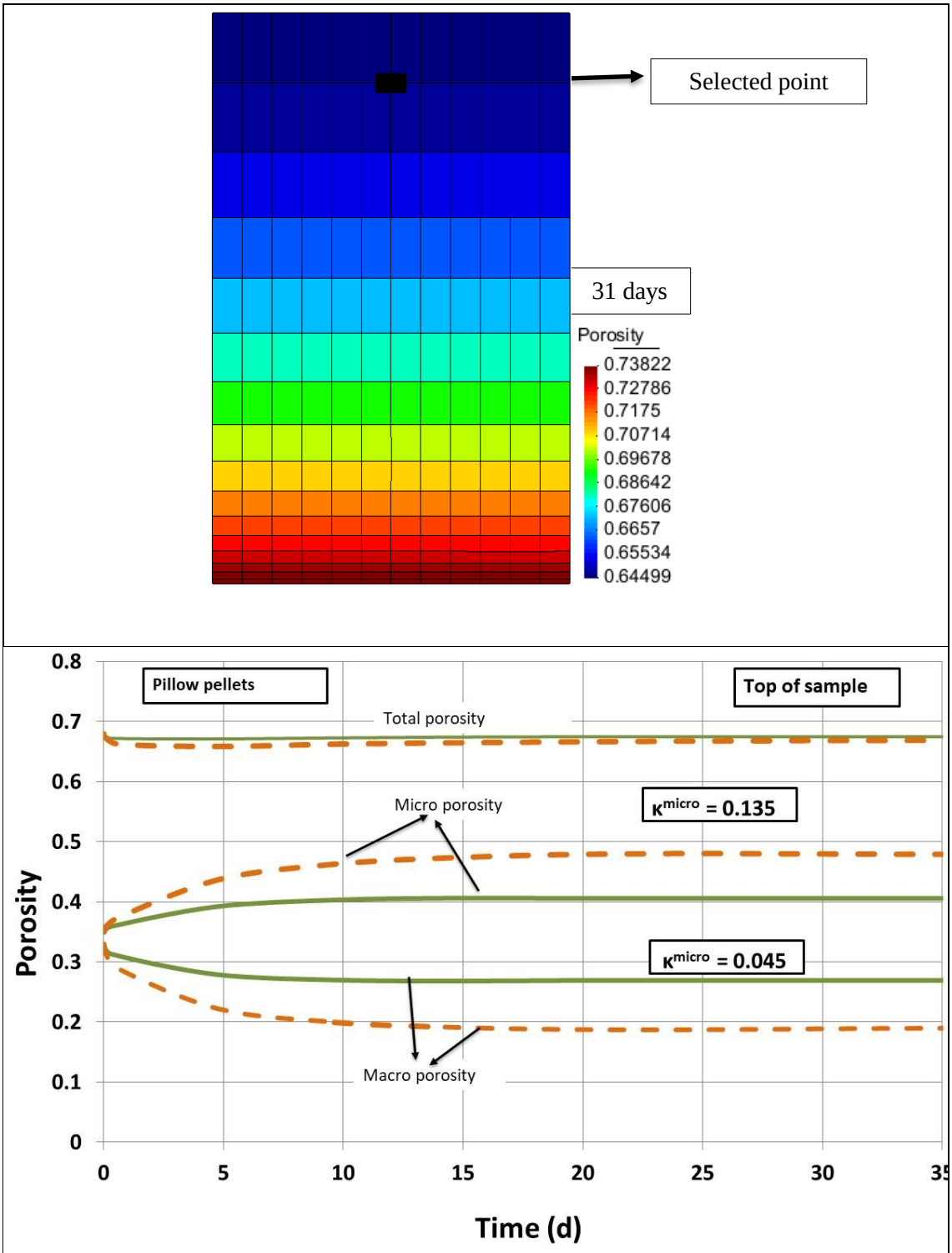

Figure 8. Calculated evolution of porosity on the top of the sample for pillow pellets, (model results). Two set of parameters (κ^{micro}=0.045 and κ^{micro}=0.135) are subjected to sensitivity analysis.

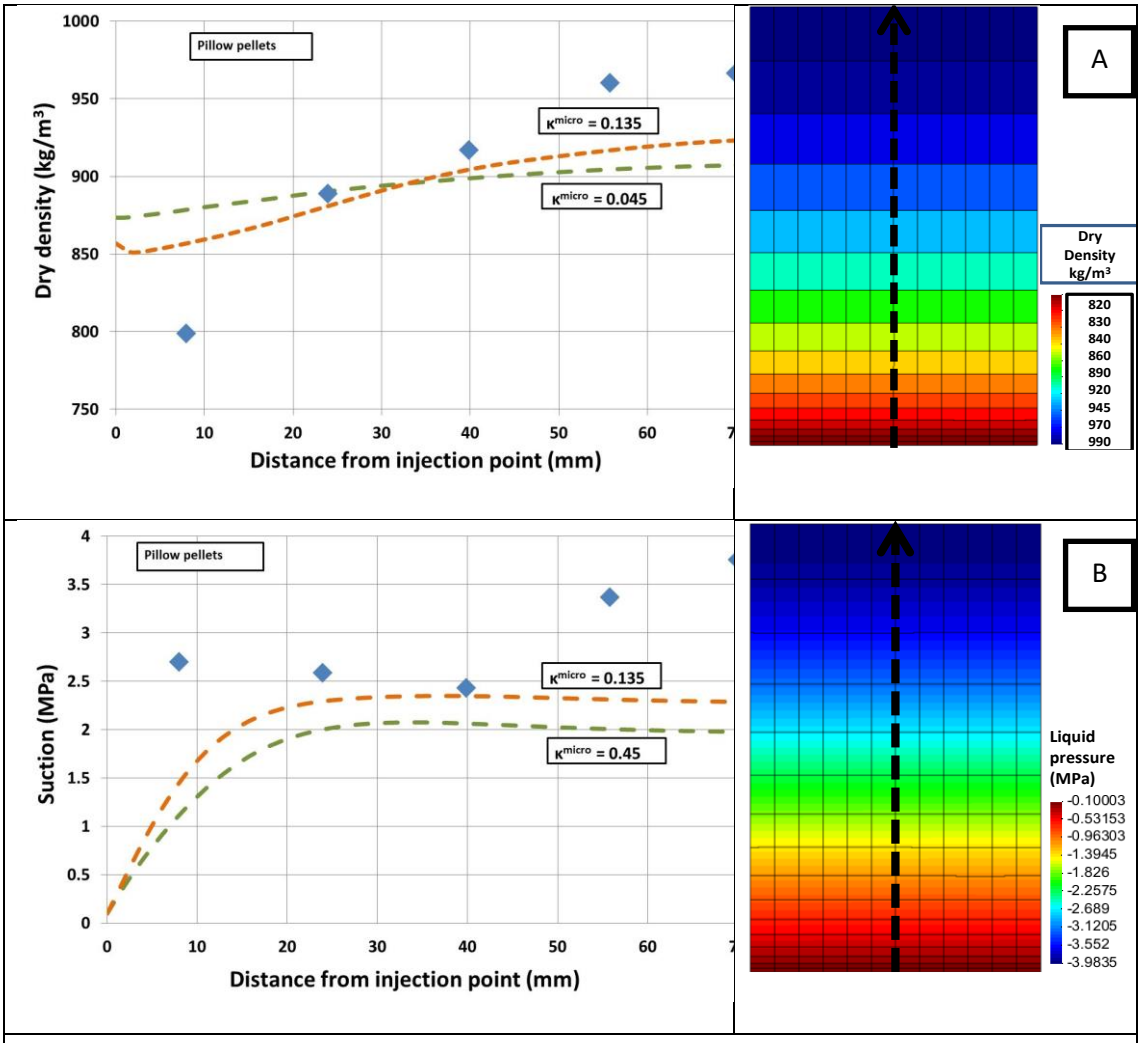

Figure 9. Distribution of dry density (A) and suction (B) as a function of distance from injection point for pillow pellets at the end of the test: 31 days, Two set of parameters (κ^{micro}=0.045 and κ^{micro}=0.135) are subjected to sensitivity analysis (experimental and model results).

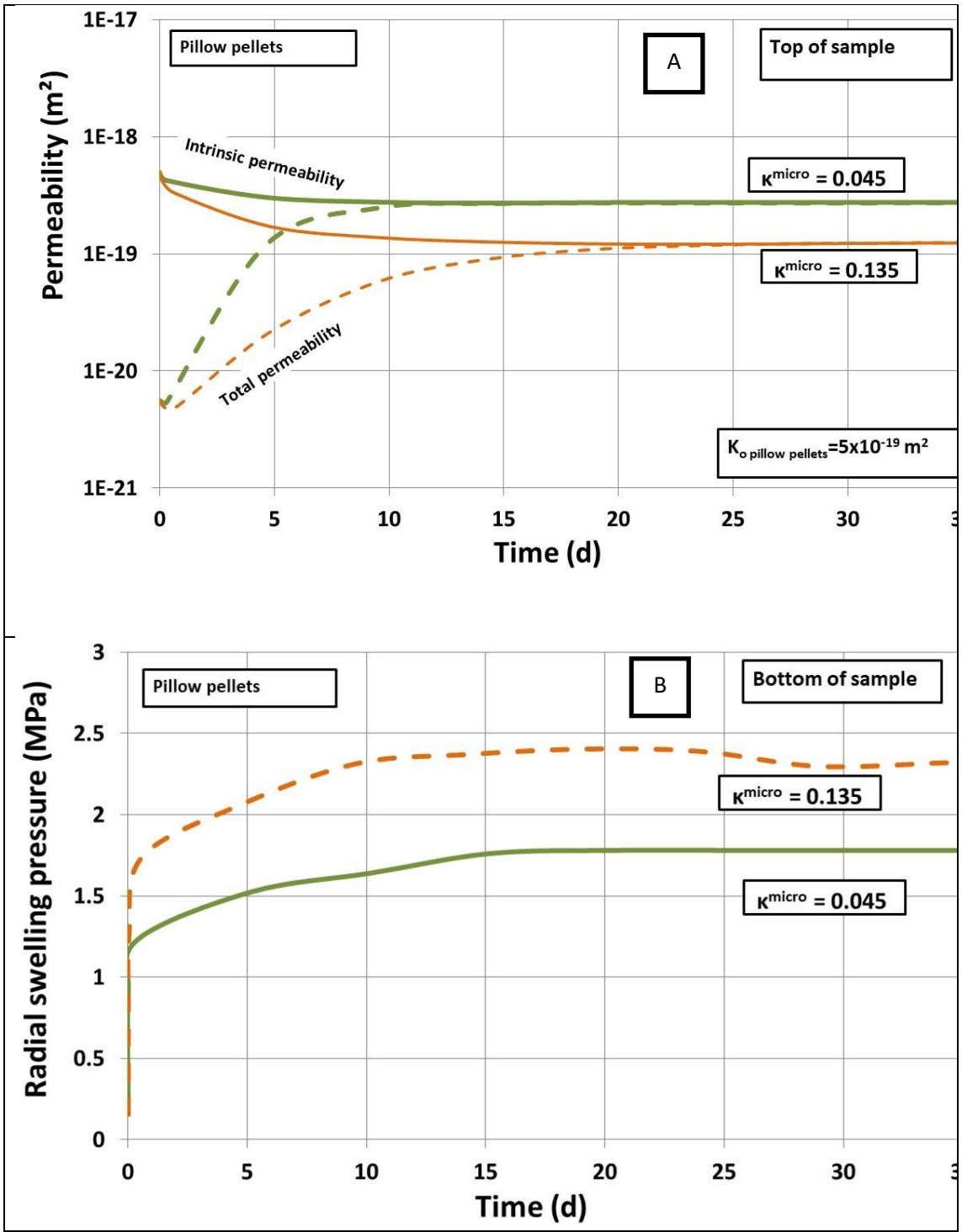

Figure 10. Evolution of permeability (A) and radial stress (B) for infiltration tests on pillow pellets, (model results Two set of parameters (κ^{micro}=0.045 and κ^{micro}=0.135) are subjected to sensitivity analysis.

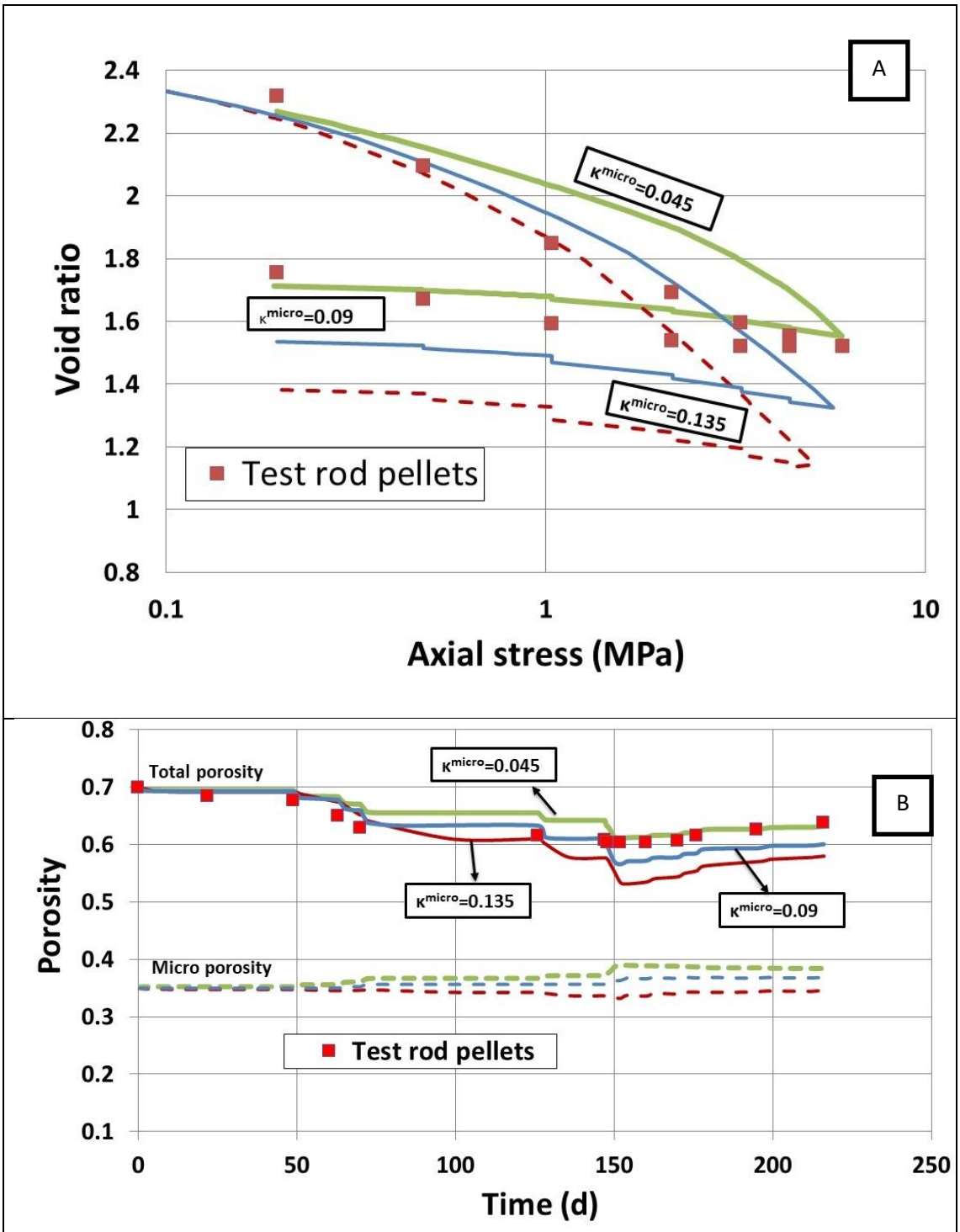

Figure 11. Void ratio vs. axial stress (A) and evolution of total, macro and micro porosity (B) for rod pellets, three set of parameters (κ^{micro}=0.045; κ^{micro}=0.09 and κ^{micro}=0.135) are subjected to sensitivity analysis (experimental and model results).

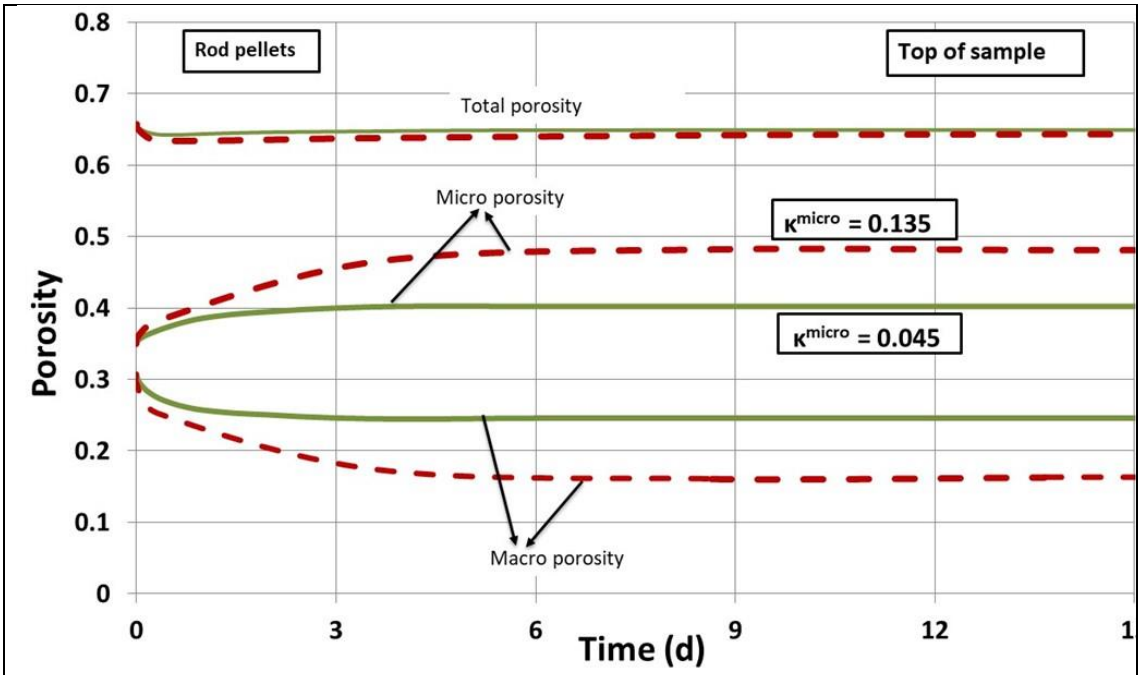

Figure 12. Evolution of porosity at the top of the sample for rod pellets (model results). Two set of parameters (κ^{micro}=0.045 and κ^{micro}=0.135) are subjected to sensitivity analysis.

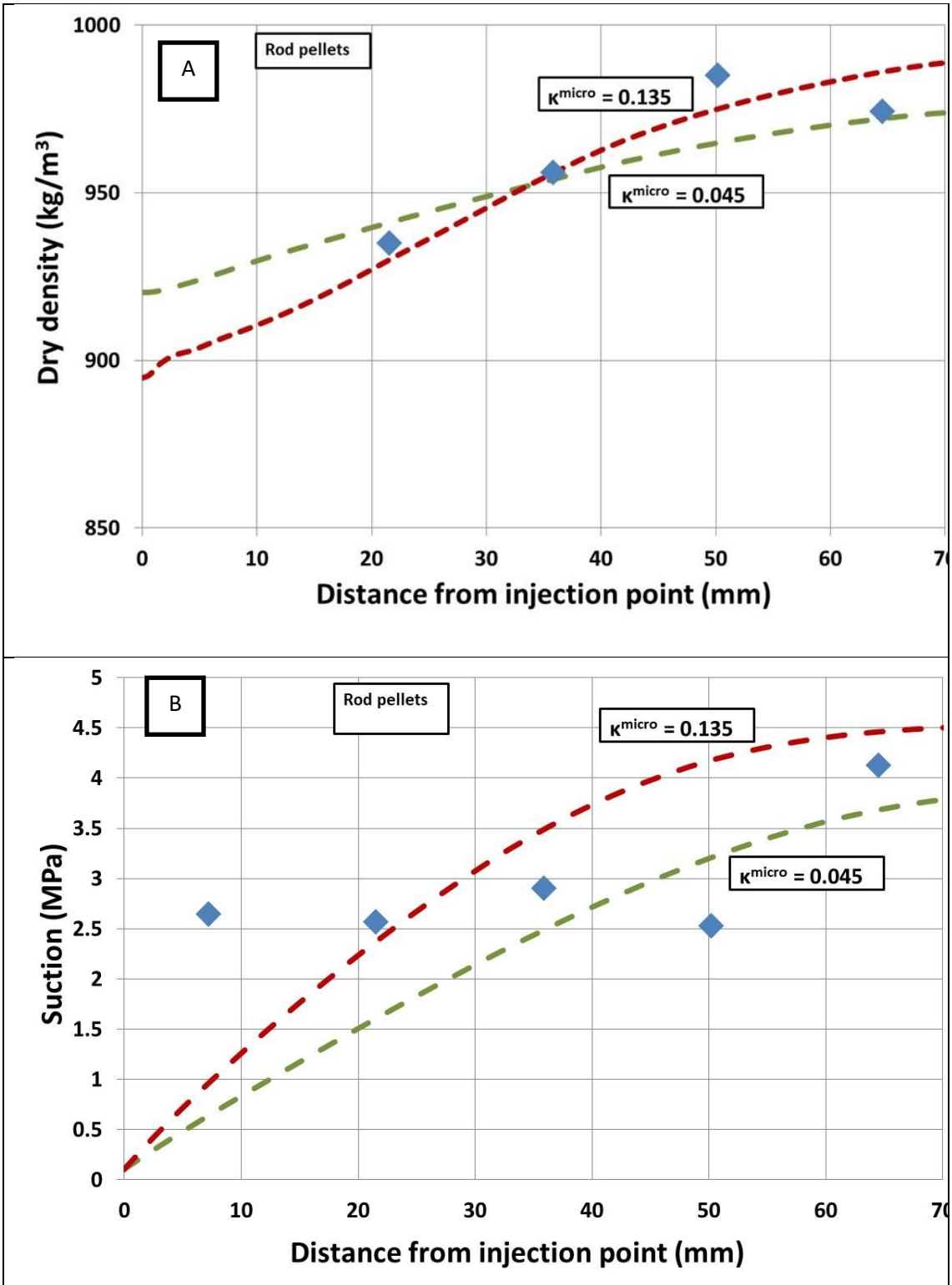

Figure 13. Distribution of dry density (A) and suction (B) as a function of distance from injection point for rod pellets at the end of the test: 15 days, Two set of parameters (κ^{micro}=0.045 and κ^{micro}=0.135) are subjected to sensitivity analysis (experimental and model results).

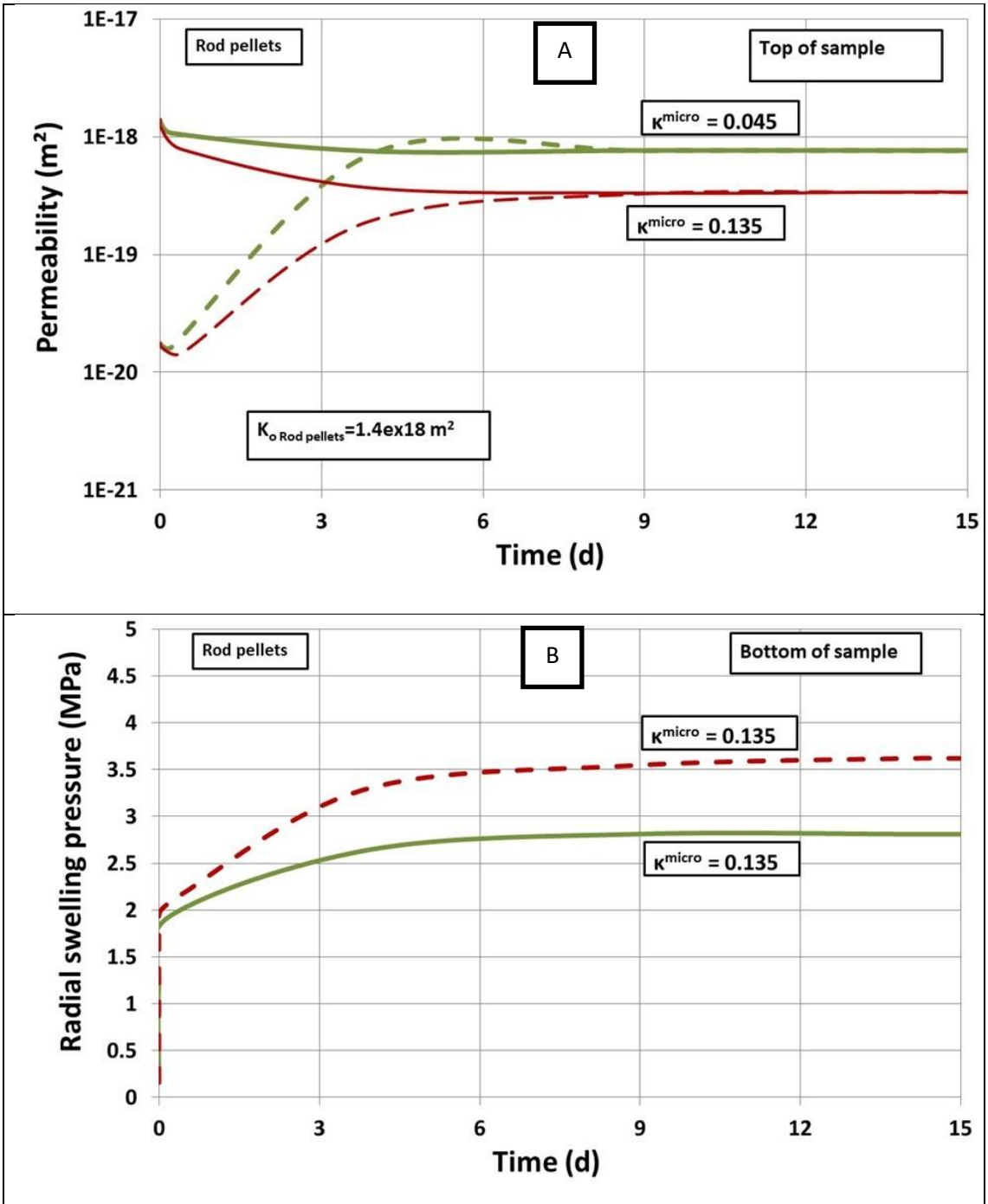

Figure 14. Evolution of permeability (A) and radial stress (B) for infiltration tests on rod pellets, (model results). Two set of parameters (κ^{micro}=0.045 and κ^{micro}=0.135) are subjected to sensitivity analysis.

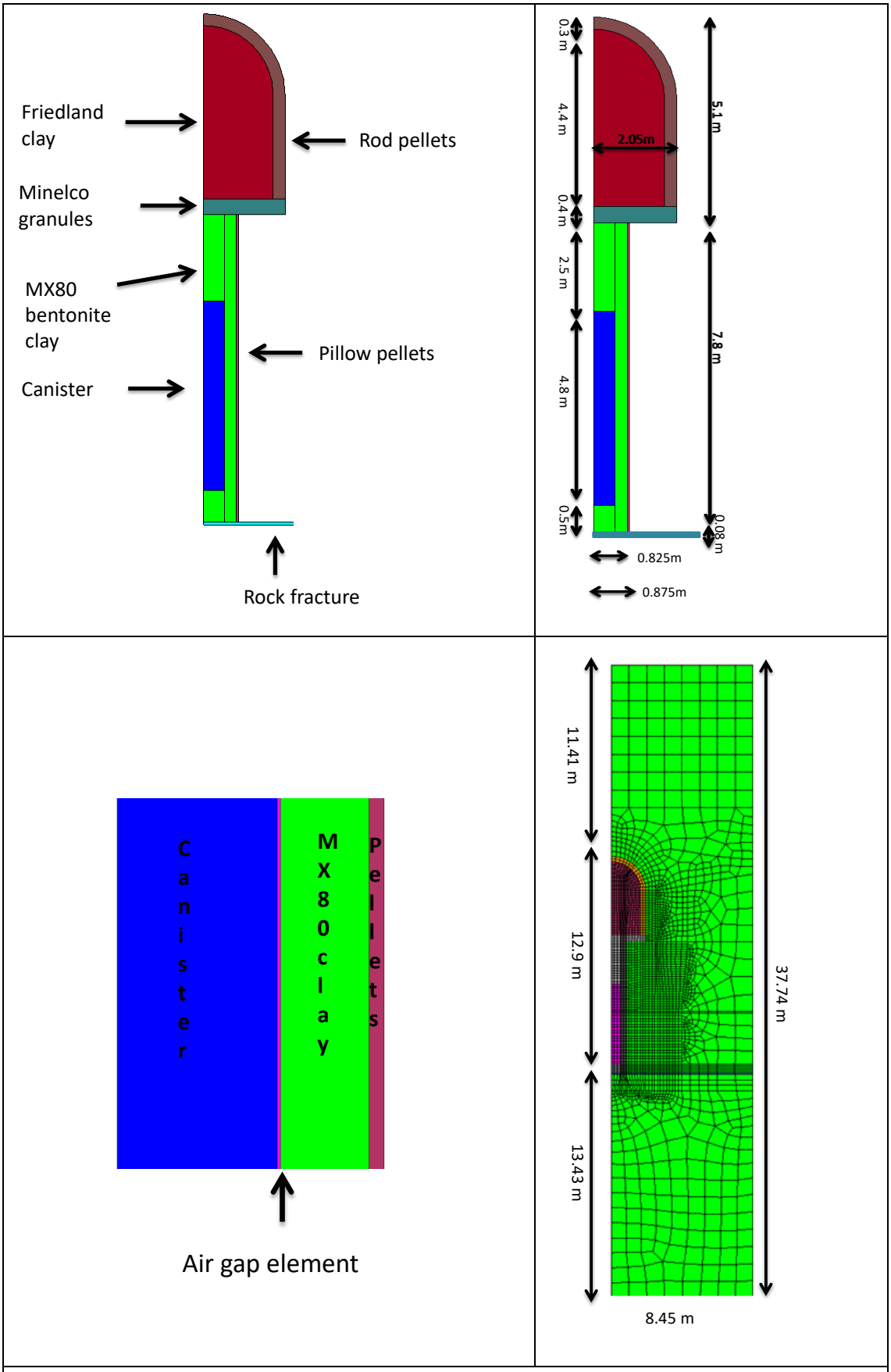

Figure 15. Materials, geometry and mesh for the model

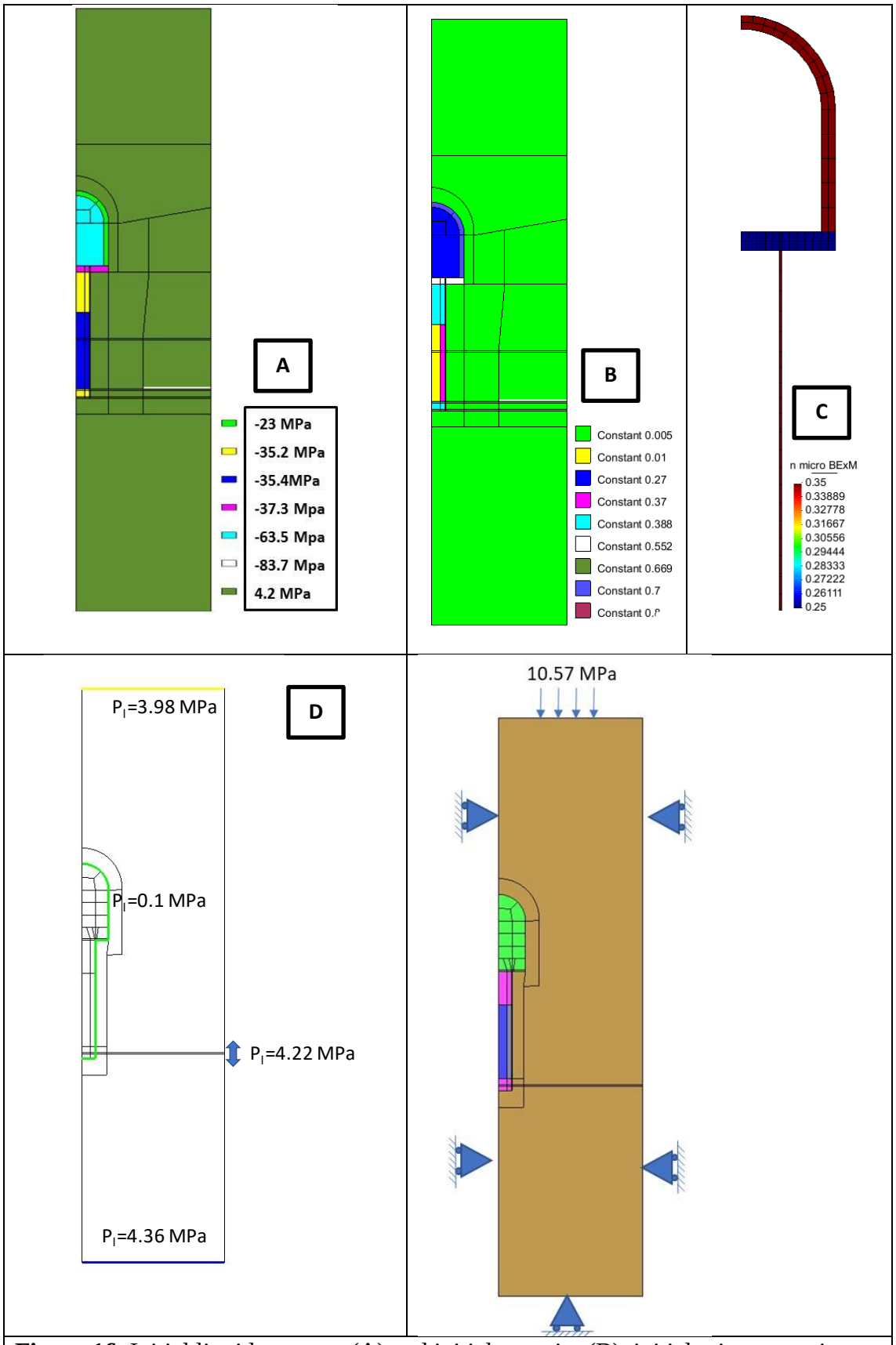

Figure 16. Initial liquid pressure (A) and initial porosity (B), initial micro porosity (C); hydraulic (D) and mechanical (E) boundary conditions for model.

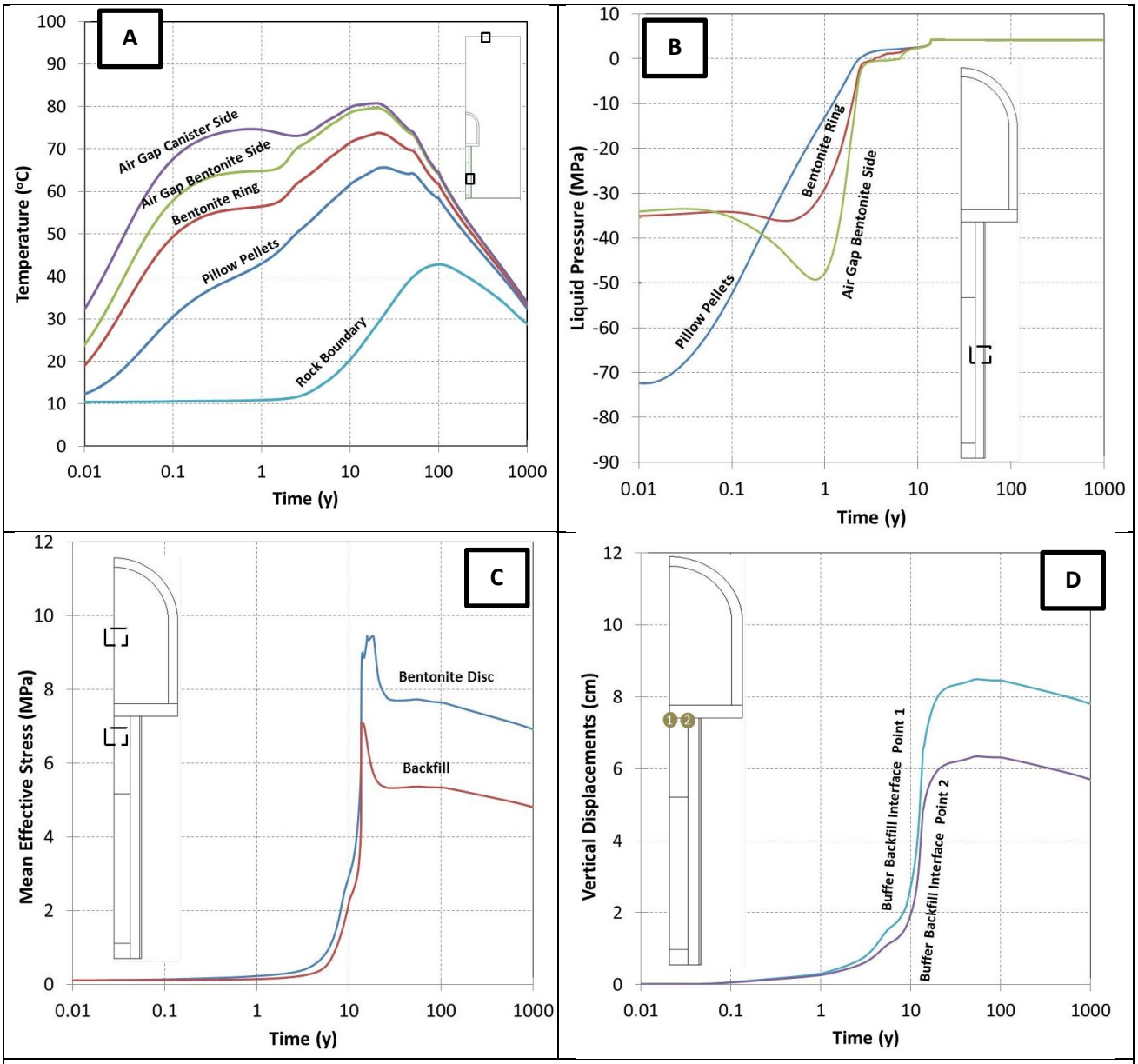

Figure 17. Evolution of tempreature (A), liquid pressure (B), mean effective stress (C) and vertical displacements (D) (model results).

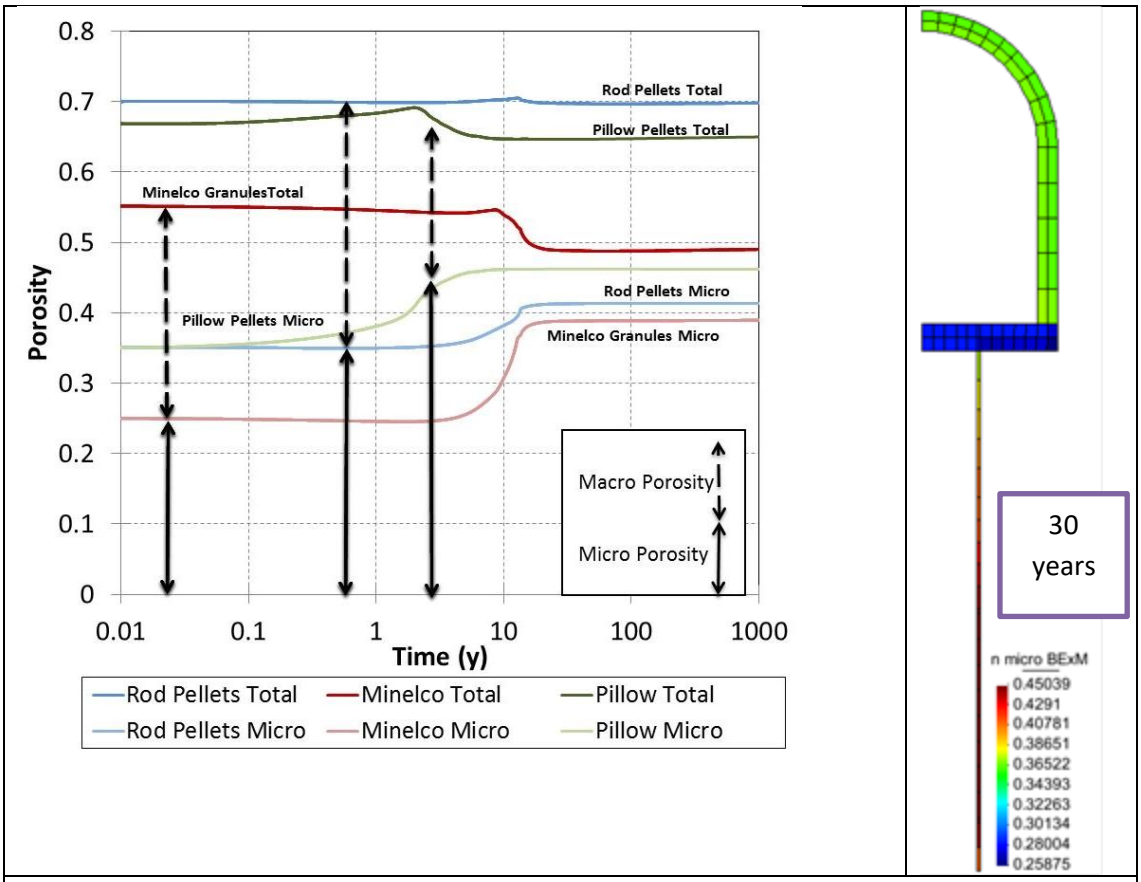

Figure 18. Evolution of micro, macro and total porosity for pellets (model results).

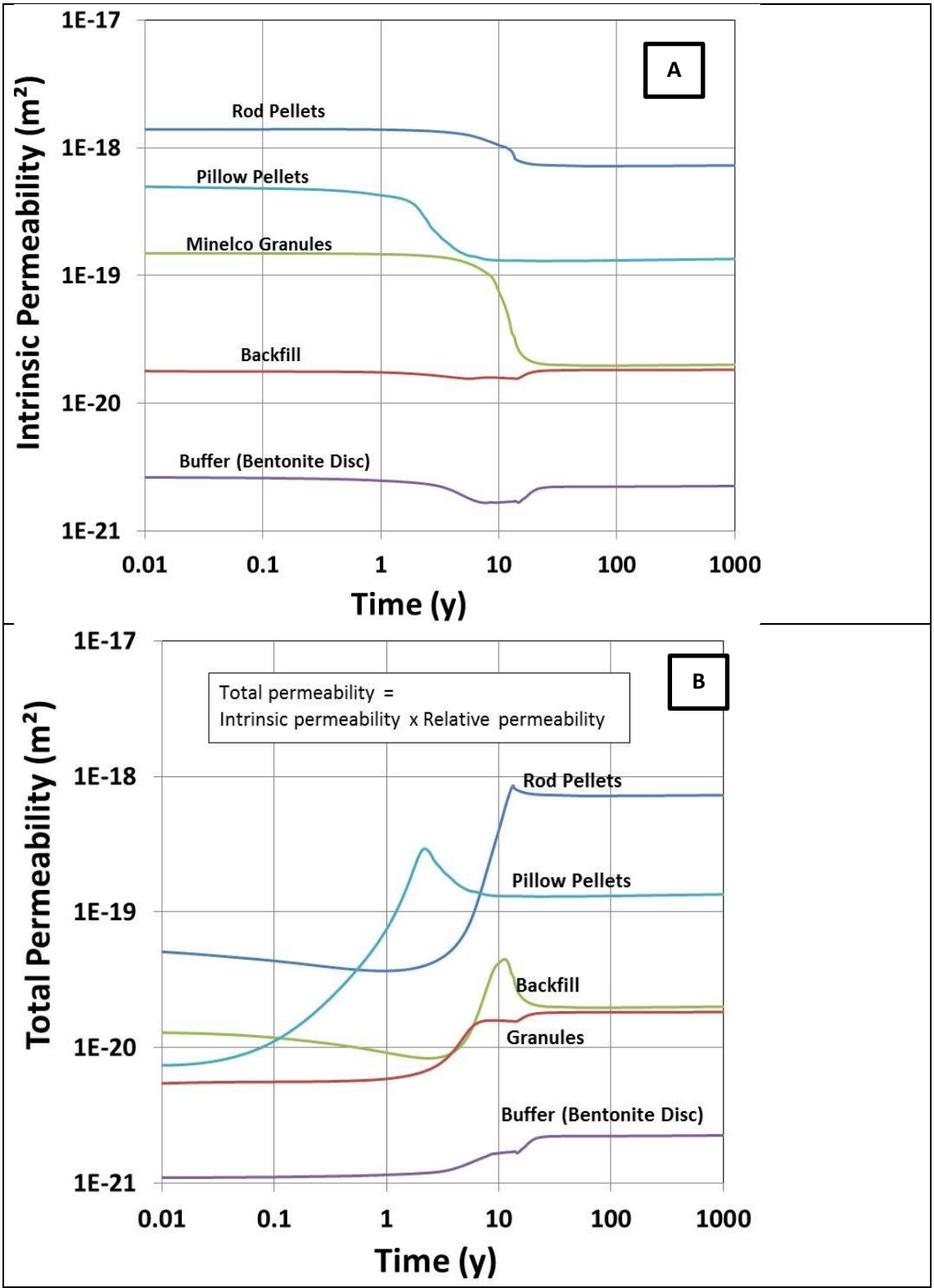

Figure 19. Evolution of intrinsic permeability (A) and total permeability (B) for clay based materials (model results).